Reconstructing past variations in environmental conditions and paleoproductivity over the last ~8000 years off north-central Chile (30° S)

Práxedes Muñoz[1,2], Lorena Rebolledo[3,4], Laurent Dezileau[5], Antonio Maldonado[2,6], Christoph Mayr[7,8], Paola Cárdenas[5,9], Carina B. Lange[4,10,11], Katherine Lalangui[10], Gloria Sanchez[12], Marco Salamanca[10], Karen Araya[1,13], Ignacio Jara[2], Gabriel Vargas[14], Marcel Ramos[1,2].

[1]Departamento de Biología Marina, Universidad Católica del Norte, Larrondo 1281, Coquimbo, Chile.
[2]Centro de Estudios Avanzados en Zonas Áridas (CEAZA), Coquimbo-La Serena, Chile.
[3]Departamento Científico, Instituto Antártico Chileno, Punta Arenas, Chile
[4]Centro FONDAP de Investigación Dinámica de Ecosistemas Marinos de Altas Latitudes (IDEAL), Universidad Austral de Chile, Campus Isla Teja, Valdivia, Chile.
[5]Normandie University, UNICAEN, UNIROUEN, CNRS, M2C, 14000 Caen, France.
[6]Instituto de Investigación Multidisciplinario en Ciencia y Tecnología, Universidad de La Serena, La Serena, Chile.
[7]Institut für Geographie, FAU Erlangen-Nürnberg, 91058 Erlangen, Germany.
[8]Department of Earth and Environmental Sciences & GeoBio-Center, LMU Munich, 80333 Munich.
[9]Programa Magister en Oceanografía, Universidad de Concepción, casilla 160C, Concepción, Chile.
[10]Departamento de Oceanografía, Facultad de Ciencias Naturales y Oceanográficas, Universidad de Concepción, Casilla 160C, Concepción, Chile.
[11]Centro de Investigación Oceanográfica COPAS Sur-Austral, Universidad de Concepción, Casilla 160C, Concepción, Chile.
[12]Universidad de Magallanes, Punta Arenas, Chile.
[13]Laboratoire Géosciences Montpellier (GM), Université de Montpellier, 34095 Montpellier Cedex 05, France.
[14]Departamento de Geología, Universidad de Chile, Santiago, Chile.

Correspondence to: Práxedes Muñoz (praxedes@ucn.cl)

Abstract

The aim of this project was to establish past variations of the main oceanographic and climatic features of a transitional semi-arid ecosystem in the north-central Chilean coast. We analyzed recent sedimentary records retrieved from two bays, Guanaqueros and Tongoy (29−30°S), for geochemical and biological analyses including: sensitive redox trace elements, biogenic opal, total organic carbon (TOC), diatoms, stable isotopes of organic carbon and nitrogen. Three remarkable periods were established, with different environmental conditions and productivities: (1) > cal BP 6500, (2) cal BP 6500 – cal BP 1700 and (3) cal BP 1700 towards the present (CE 2015). The first period was characterized by a remarkably higher productivity (higher diatom abundances and opal) when large fluxes of organic compounds were also inferred from the accumulation of elements such as Ba, Ca, Ni, Cd and P in the sediments. At the same time, suboxic-anoxic conditions at the bottoms were suggested by the large accumulation of Mo, Re and U, showing a peak at cal BP 6500, when sulfidic conditions could have been established. This was also identified as the driest interval according to the pollen moisture index. These conditions should be associated to an intensification of the SPSA and a stronger SWW, emulating La Niña-like conditions as has been described for the SE Pacific during the early Holocene, which in this case extends until the mid-Holocene. During most of the second period, lower productivity was observed. However, a small increment was identified between Cal BP 4500 and 1700, although low amounts of diatom (valves g^{-1}) and nutrient-type metal accumulations were observed. Oxygen conditions at the bottoms change to an almost stable sub-oxic condition during this time interval. The third period is marked by an intense oxygenation after cal BP 1700, as observed by a change in the accumulation of U, Mo and Re. In Addition, a small productivity rise after cal BP ~130 towards recent times was observed, as suggested by opal accumulations but no increment in diatom abundance. Overall, lower primary productivity, higher oxygenation at bottoms, and higher humidity conditions were established after cal BP 6500 and towards the present. We suggest that the oxygenation might be associated with an intensified El Niño activity or similar conditions that introduce oxygenated waters to coastal zones by the propagation of waves of equatorial origin, and establishing conditions that have reduced the primary productivity from the mid Holocene toward the beginning of modern era.

Keywords: paleoproductivity, paleoredox, trace metals, diatoms, opal, organic carbon, Coquimbo, SE-Pacific

1. Introduction

The mean climatic conditions at the SE Pacific are modulated by the dynamic of the Southern Pacific Subtropical Anticyclone (SPSA) and the Humboldt Current System. The SPSA has seasonal, decadal, and inter-decadal variability modulating the strength of the southern westerly winds (SWW) and hence, the main oceanographic feature of the Eastern boundary margin, the upwelling, influencing the biogeochemical processes related to the inputs of nutrient and biological productivity. Seasonal variations produce periods of intense upwelling when the SPSA is stronger, while the opposite is true when it is weak (Croquette et al, 2007). The coastal wind pattern produced alongshore varies along the SE Pacific showing lower seasonality between 18°−30°S, and producing a semi-permanent upwelling (Pizarro et al., 1994; Figueroa and Moffat, 2000). This system is highly affected by the inter-annual variability imposed by El Niño Southern Oscillation (ENSO), with impacts on the wind intensity. The upwelling brings nutrient-poor waters during the warm phase, while the opposite happens during the cold phase (Ruttland and Fuenzalida, 1991; Blanco et al., 2002). Other climate patterns −namely the Pacific Decadal Oscillation (PDO) and the Southern Annular Mode (SAM)− operate on a much longer time scale (inter-annual, decadal, inter-decadal) modifying the strength and the position of the SWW, and thereby producing cold/warm periods affecting mainly winter precipitations during positive/negative trends of SAM and leading to intense/weak upwelling (Quintana and Aceituno, 2012; Ancapichún and Garcés-Vargas, 2015). In addition, the orbitally induced austral insolation influences the extent of the Antarctic sea ice and the Hadley cell, which act as important forces to the latitudinal displacement of the ITCZ (Inter-tropical Convergence Zone; Kaiser et al., 2008, and references therein). These fluctuations produce humid and arid conditions along the SE Pacific where the wind’s intensity remains the key factor for the upwelling’s strength and, therefore, for the supply of nutrients to the photic zone, all of which are required for the development of the primary productivity.

Off Coquimbo (30°S), there is normally a semi-permanent and intense upwelling forced by local winds, strongly influenced by topographic features (Figueroa and Moffat, 2000) and ENSO variability (Schaffer et al., 1997; Escribano et al., 2004). During El

Niño, mean winds alongshore reduce their intensity and the South East Pacific anticyclone weakens. Conversely, during La Niña mean winds alongshore increase their intensity and the anticyclone is reinforced (Rahn and Garreaud, 2013). This has an impact on the upper circulation of the ocean affecting the oxygenation of the water column and the strength of upwelling. The high productivity that takes place close to the coast during normal periods (Escribano et al., 2004 and references therein) maintains a zone of low dissolved oxygen content along the margin reinforcing the oxygen minimum zone (OMZ). This zone develops along the North and South Pacific Ocean and its intensity, thickness, and temporal stability vary as a function of latitude (Helly and Levin, 2004, Ulloa et al., 2012). To the north (e.g. 21°S) and off Peru, the OMZ occurs permanently, and can extend into the euphotic zone. In the case of northern Chile and southern Peru, there is no significant interface with the benthic environment due to the presence of a narrow continental shelf (Helly and Levin, 2004). The OMZ dynamic off Coquimbo has not been studied in detail, but a seasonal intrusion of low oxygen waters to the coast has been observed (Gallardo et al., 2017). During the 97-98 El Niño event, the oxygenation of bottoms was clearly detected in north (23°S) and south-central Chile (36°S) (Ulloa et al., 2001; Gutiérrez et al., 2006; Sellanes et al., 2007), changing the normal suboxic conditions at the bottom, the normal composition of macrofauna and related geochemical characteristics of the sediments having implications that persist for many years after the event (Gutiérrez et al., 2006; Sellanes et al., 2007).

These changes in primary productivity and oxygenation at the bottom can be observed in sedimentary records which respond to the amount of organic carbon that has settled on the surface sediments and to the diagenetic reactions during organic matter remineralization. Trace elements are commonly used as indicators of these processes, observed as element enrichment or depletion. They are driven by organic matter fluxes and redox conditions that modify the original extension of metal enrichment, which depend on the oxygen content during early diagenesis in the upper sediment layers and overlying water (Nameroff et al., 2002; Zheng et al., 2002; McManus et al., 2006; Siebert et al., 2003). Therefore, they are a useful tool to establish temporary changes in primary productivity and also to establish changes in the oxygenation at the bottom on sedimentary records.

Our work focuses on the past variations of the environmental conditions deduced from marine sedimentary records of inorganic and organic proxies over the last ~8000 years

BP, obtained from a transitional semiarid ecosystem off the central Chilean coast (30°S), close to Lengua de Vaca point, the most relevant upwelling area of Chile's northern margin (Shaffer et al., 1999; Thiel et al., 2007). We considered redox trace element measurements that respond to local hypoxia (U, Mo and Re), as well as nutrient-type elements that follow the organic fluxes to the sediments (Ba, Ni Cu, P) (Tribovillard, 2006). Additionally, we measured Fe and Mn which play a key role in adsorption-desorption and scavenging processes of dissolved elements in bottom waters and sediments, and we measured Ca, K and Pb used to assess terrigenous inputs by coastal erosion, weathering and eolian transport, which is also true for Fe and Mn (Calvert and Pedersen, 2007). Ca accumulation depends, in turn, on carbonate productivity and dissolution, which has been used as a paleoproductivity proxy (Paytan, 2008; Govin et al., 2012). We determined the enrichment/depletion of elements to establish the main environmental conditions prevailing during the sedimentation of particulate matter (Böning et al., 2009). In addition, we considered the diatom assemblages with biogenic opal as a measurement of siliceous export production, TOC, and stable isotopes to identify variations in the organic fluxes to the bottoms. Moreover, pollen grains were used to identify environmental conditions based on the climate relationship of the main vegetation formations in North-Central Chile. Based on our records we were able to identify wet/dry intervals, periods with high/low organic fluxes to the sediments related to changes in primary production, and changes in the redox conditions at the bottoms.

2. Study area

The Coquimbo area (29-30°S) −in the southern limit of the northern-central Chilean continental margin− constitutes a border area between the most arid zones of northern Chile (Atacama Desert) and the more mesic Mediterranean climate in central Chile (Montecinos et al., 2016). Here, the shelf is narrow and several small bays trace the coast line.

The Tongoy and Guanaqueros bays are located in the southern edge of a broad embayment between small islands to the north (29°S; Choros, Damas and Chañaral) and Lengua de Vaca Point to the south (30°S) (Fig. 1), protected from predominant southerly winds. Tongoy Bay is a narrow marine basin (10 km at its maximum width) with a maximum depth of ~100 m. To the northeast lies Guanaqueros Bay, a smaller and shallower basin. High wind events evenly distributed throughout the year promote an important upwelling center at Lengua de Vaca Point, developing high biomass along a narrow coastal area (Moraga-Opazo et al., 2011; Rahn and Garreaud, 2013), and reaching maximum concentrations of ~20 mg m^{-3} (Torres and Ampuero, 2009). In the shallow waters of Tongoy Bay, the high primary productivity results in high TOC in the water column allowing for the deposition of fine material to the bottom; TOC rises concurrently with the periods of low oxygen conditions (Fig. 2; Muñoz et al., unpublished data). Recent oceanographic studies indicate that low dissolved oxygen water intrusions from the shelf (Fig. 3) seem to be related to lower sea levels resulting from annual local wind cycles at a regional meso-scale (Gallardo et al., 2017). Oceanographic time series indicate that transition times develop in short periods due to changes in the directions and intensities of the winds along the coast, with a strong seasonality (http://www.cdom.cl/boyas-oceanograficas/boya-tongoy). The spatial and temporal variability of these processes is still under study. In addition, oceanic variability along the western coast of South America is influenced by equatorial Kelvin waves on a variety of timescales, from intra-seasonal (Shaffer et al.,1997) and seasonal (Pizarro et al., 2002; Ramos et al., 2006), to inter-annual (Pizarro et al., 2002; Ramos et al., 2008). Coastal-trapped Kelvin waves originating from the equator can propagate along the coast, modifying the stability of the regional current system and the pycnocline, and triggering extra-tropical Rossby waves (Pizarro et al., 2002; Ramos et al., 2006; 2008). This oceanographic feature will change the oxygen content in the bays with major impacts on redox-sensitive elements in the surface sediments.

Sedimentological studies are scarce in Chile's northern-central shelf. A few technical reports indicate that sediments between 27°S and 30°S are composed of very fine sand and silt with relatively low organic carbon content (<3 and ~5%), except in very limited coastal areas where organic material accounts for approximately ~16% (Muñoz, unpublished data; FIP2005-61 Report, www.fip.cl). Coastal weathering is the main source of continental input due to scarce river flows and little rainfall in the zone (0.5 to ~80 mm yr^{-1}; Montecinos et al., 2016, Fig.1). Freshwater discharges are represented by creeks, which receive the drainage of the coastal range forming wetland areas in the coast and even small estuaries, such as Pachingo, located south of Tongoy (Fig. 1). These basins cover ~300 and 487 km^2, respectively. The water volume in the estuaries is maintained by the influx of seawater mixed with groundwater supply. No surface flux to the sea is observed. Therefore, freshwater discharge occurs only during high rainfall periods in the coastal zone (DGA, 2011), which normally takes place during El Niño years when higher runoff has been recorded in the area during the austral winter (Valle-Levinson et al., 2000; Montecinos and Aceituno, 2003; Garreaud et al., 2009). Under this scenario, marine sediments are often highly influenced by primary production in the water column, terrestrial runoff, and therefore, sedimentary records can reveal past variability in primary production and in the oceanographic conditions over the shelf, which ultimately respond to major atmospheric patterns in the region.

3. Materials and methods

3.1. Sampling

Sediment cores were retrieved from two bays in the Coquimbo region: Bahía Guanaqueros (core BGGC5; 30°09' S, 71°26' W; 89 m water depth) and Bahía Tongoy (core BTGC8; 30°14' S, 71°36' W; 85 m water depth) (Fig. 1.), using a gravity corer (KC-Denmark) during May 2015, on board the L/C Stella Maris II owned by the Universidad Católica del Norte. The length of the cores was 126 cm for BGGC5 and 98 cm for BTGC8.

Subsequently, the cores were sliced into 1-cm sections and subsamples were separated for grain size measurements, magnetic susceptibility, trace elements, biogenic opal, C and N stable isotope signatures ($\delta^{13}C$, $\delta^{15}N$), and TOC analyses. The samples were first kept frozen (–20° C) and then freeze-dried before laboratory analyses.

3.2. Geochronology (^{210}Pb and ^{14}C)

Geochronology was established combining ages estimated from $^{210}Pb_{xs}$ activities suitable for the last 200 years and radiocarbon measurements at selected depths for older ages. ^{210}Pb activities were quantified through alpha spectrometry of its daughter ^{210}Po following the procedure of Flynn (1968). $^{210}Pb_{xs}$ (unsupported) activities were determined as the difference between ^{210}Pb and ^{226}Ra activities measured in some intervals of the sediment column. ^{226}Ra was measured by gamma spectrometry at the Laboratoire Géosciences of the Université de Montpellier (France). Standard deviations (SD) of the ^{210}Pb inventories were estimated propagating counting uncertainties (Bevington and Robinson, 1992) (Table S1, supplementary data). The ages were based on the Constant Rate of Supply Model (CRS, Appleby and Oldfield, 1978).

Radiocarbon measurements were performed on a mix of planktonic foraminifer species in core BGGC5 whereas the benthic foraminifer species *Bolivina plicata* was selected for core BTGC8 (Table 1). The samples were submitted to the National Ocean Sciences

AMS Facility (NOSAMS) of the Woods Hole Oceanographic Institution (WHOI). The time scale was obtained according to the best fit of ages obtained from $^{210}Pb_{xs}$ and ^{14}C (Fig. 4), using the CLAM 2.2 software and using the Marine curve 13C (Reimer et al., 2013). A reservoir deviation from the global mean reservoir age (DR) of 441 ± 35 years was considered, established according Sabatier et al. (2010). This was estimated subtracting the 14C age value corresponding at the historical dates 1828 AD and 1908 AD (499 ± 24 and 448 ± 23 ^{14}C yr, respectively, Reimer et al., 2013) from the apparent ^{14}C age of foraminifers measured at depths of 5 and 10 cm for cores BTGC8 and BGGC5, respectively (Sabatier et al., 2010; Table 2).

3.3. Geophysical characterization

Magnetic susceptibility ($SIx10^{-8}$) was measured with a Bartington Susceptibility Meter MS2E surface scanning sensor at the Sedimentology Laboratory at Centro Eula, Universidad de Concepción. Mean values from three measurements were calculated for each sample.

Grain size was determined using a Mastersizer 2000 laser particle analyzer, coupled to a Hydro 2000−G Malvern in the Sedimentology Laboratory of Universidad de Chile. Skewness, sorting and kurtosis were evaluated using the GRADISTAT statistical software (Blott and Pye, 2001), which includes all particle size spectra.

3.4. Chemical analysis

Trace element analyses were performed by ICP-MS (Inductively Coupled Plasma-Mass Spectrometry) using an Agilent 7700x at Université de Montpellier (OSU OREME/AETE regional facilities). The analysis considered reference materials (UBN, BEN and MAG1) obtaining an accuracy higher than ±5%; the analytical precisions were between 1% and 3%. Internal standardizations with In and Bi were used to deconvolve mass-dependent sensitivity variations of both matrix and instrumental origin, occurring during the course of an analytical session. The analytical precisions attained were between 1% and 3%.

TOC and stable isotope ($\delta^{15}N$ and $\delta^{13}C$) analyses were performed at the Institut für Geographie, Friedrich Alexander Universität (FAU) Erlangen-Nürnberg, Germany using a Carlo Erba elemental analyzer NC2500 and an isotope-ratio-mass spectrometer (Delta Plus, Thermo-Finnigan) for isotopic analysis. Stable isotope ratios are reported in the δ notation as the deviation relative to international standards (Vienna Pee Dee

Belemnite for $\delta^{13}C$ and atmospheric N_2 for $\delta^{15}N$), so $\delta^{13}C$ or $\delta^{15}N$ = [(R sample/R standard) − 1] x 10^3, where R is $^{13}C/^{12}C$ or $^{15}N/^{14}N$, respectively. Typical precision of the analyses was ±0.1‰ for $\delta^{15}N$ and $\delta^{13}C$.

Biogenic opal was estimated following the procedure described by Mortlock and Froelich (1989). The analysis was done by molybdate-blue spectrophotometry (Hansen and Koroleff, 1999) conducted at the laboratories of Marine Organic Geochemistry and Paleoceanography, University of Concepción, Chile. Values are expressed as biogenic opal by multiplying the Si (%) by 2.4 (Mortlock and Froelich, 1989). Analytical precision was ± 0.5%. Accumulation rates were determined based on sediment mass accumulation rates and amount of opal at each core section in %.

3.5. Microfossils analyses

Qualitative abundances of siliceous microfossils were carried out every one centimeter following the Ocean Drilling Program (ODP) protocol, described by Mazzullo and Graham (1988). This information was used to select some sections every ~4, 8 and 12 cm for BGGC5 and at ~6 cm for BTGC8, for quantitative abundances of microfossils (diatoms, silicoflagellates, sponge spicules, crysophyts and phytoliths). Roughly ~ 0.5 g of freeze-dried sediment was treated according to Schrader and Gersonde (1978) for siliceous microfossils. They were identified and counted under an Olympus CX31 microscope with phase contrast. 1/5 of the slides were counted at 400X for siliceous microfossils and one transect at 1000x was counted for *Chaetoceros* resting spores (*Ch.* resting spores). Two slides per sample were counted; the estimated counting error was 15%. Total diatom abundances are given in valves g^{-1} of dry sediments.

Pollen analysis was conducted following the standard pollen extraction methodology (Faegri and Iversen, 1989). The identification was conducted under a stereomicroscope, with the assistance of the Heusser (1973) pollen catalogue. A total of 100-250 terrestrial pollen grains were counted in each sample. Pollen percentage for each taxon was calculated from the total sum of terrestrial pollen (excluding aquatic taxa and fern spores). Pollen percentage diagrams and zonation were generated using the Tilia software (Grimm, 1987).

We further summarize pollen-based precipitation trends by calculating a Pollen Moisture Index (PMI), which is defined as the normalized ratio between Euphorbiaceae (wet coastal scrubland) and Chenopodiaceae (arid scrubland). Thus, positive (negative) values of this index point to relatively wetter (drier) conditions.

4. Results

4.1. Geochronology

$^{210}Pb_{xs}$ (unsupported activity) was obtained from the surface at a depth of 8 cm in the two cores, with an age of ~ AD 1860 at 8 cm in both (Table S1). Greater surface activities were obtained for core BGGC5 (13.48 ± 0.41 dpm g^{-1}) compared to core BTGC8 (5.80 ± 0.19 dpm g^{-1}), showing an exponential decay with depth (Fig. 4). A recent sedimentation rate of 0.11±0.01 cm yr^{-1} was estimated.

The age model provided a maximum age of cal BP 8210 for core BGGC5, and cal BP 7941 for core BTGC8 (Fig. 4). A mean sedimentation rate of 0.02 cm yr^{-1} was estimated for core BGGC5, with a period of relative low values (0.01 cm yr^{-1}) between cal BP ~4000 and 6000. For BTGC8, sedimentation rates were less variable and around 0.013 cm yr^{-1} in the entire core. An age reservoir estimation following the method by Sabatier et al. (2010) resulted in 441 ± 35 and 442 ± 27 years for BGGC5 and BTGC8 cores, respectively (Table 2). These values were close to the global marine reservoir and higher than other estimations along the Chilean margin at shallower depths (146 ± 25 years at < 30 water depth; Carré et al., 2016; Merino-Campos et al., 2018). Our coring sites are deeper (~90 m water depth) and influenced by upwelled water from Lengua de Vaca Point, which could explain such differences. However, moderate differences were observed between models using both reservoir values. Thus, our estimations were based on two pre-bomb values established with ^{210}Pb measured in sediments and ^{14}C in foraminifers, used for the age modeling.

4.2. Geophysical characterization

Sediments retrieved from the bays showed fine grains within the range of very fine sand and silt in the southern areas. There, grain size distribution was mainly unimodal, very leptokurtic, better sorted and skewed to fine grain when compared to sediments from the northern areas. Sediment cores obtained from the northern areas were sandy (coarse sand and gravel), with abundant calcareous debris. Longer cores of soft sediment were retrieved at the southernmost areas (BGGC5 and BTGC8), where the silty component varied between 40 % and 60 % (Fig. 1 and 5a,b). The clay component was very low at both cores (<2%). The sediment's color ranged from very dark grayish brown to dark olive brown (2.5Y 3/3−3/2) in Guanaqueros Bay (BGGC5) and from dark olive gray to olive gray (5Y 3/2−4/2) in Tongoy Bay (BTGC8). Visible macro-remains (snails and fish vertebrae) were found, as well as weak laminations at both cores. The magnetic susceptibility showed higher values close to the surface, up to 127 SI x10^{-8} at BGGC5, and relative lower values (85 SI x10^{-8}) at BTGC8. At greater depths, however, the values were very constant, around 5−8 x10^{-8} SI at BGGC5 core and around 12−20 x10^{-8} SI at BTGC8 core. In both cores, susceptibility rises substantially in the last century (Figs. 5a, 5b). Lower bulk densities were estimated at core BGGC5 (0.7−0.9 g cm^{-3}), compared with core BTGC8 (>1 g cm^{-3}) (Fig. 5a, 5b). In line with this, mean grain size amounted to 60−80 µm in Guanaqueros Bay (BTGC8), compared to 50−60 µm in Tongoy Bay (BGGC5). Both cores were negatively skewed, with values of -1 to -1.2 at BGGC5, and -1 to -2.5 at BTGC8. Minor increases towards coarser grain size were observed in the last ~1000 years, especially in Tongoy Bay (BTGC8). In both cases, grain size distributions were strongly leptokurtic. Ca/Fe ratio also reduced in time, except at core BTGC8 where it was only observed during the last ~2000 years.

4.3. Biogenic components

4.3.1. Siliceous microfossils and biogenic opal

Total diatom abundance fluctuated between 5.52 x10^5 and 4.48 x10^7 valves g^{-1} at core BGGC5. Total diatom abundance showed a good correlation with biogenic opal content at BGGC5 (R^2 =0.52, P<0.5), with values raising from 72 cm to the bottom of the core, corresponding to cal BP 5330, and reaching their highest values before cal BP 6500. On the contrary, diatom abundance and biogenic opal were much lower at core BTGC8 (< 2 ×10^5 valves g^{-1} and <3%, respectively). Here, the siliceous assemblage was almost completely conformed by *Chaetoceros* resting spores (RS) (Fig. 6).

A total of 135 and 8 diatom taxa were identified in cores BGGC5 and BTGC8 respectively, where core BTGC8 registered very low diatom abundances. In general, diatoms were the most important assemblage of siliceous microfossils (96 %), followed by sponge spicules (3 %). The contribution of phytoliths and chrysophyte cysts was less than 2 % at core BGGC5. *Chaetoceros* (RS) dominated diatom assemblage (~90 %; Fig. 6), and included the species *C. radicans*, *C. cinctus*, *C. constrictus*, *C. vanheurckii*, *C. coronatus*, *C. diadema*, and *C. debilis*. Other upwelling group species recorded (mainly at core BGGC5) were: *Skeletonema japonicum*, and *Thalassionema nitzschioides* var. *nitzschioides* (Table S2). Other species range from ~0.3% to 6 % of the total assemblage.

4.3.2. TOC and stable isotopes distribution

Consistent with opal and diatoms, core BGGC5 showed higher values of TOC (between 2 % and 5 %) compared with less than ~1.5 % at core BTGC8 (Fig. 5a,b). Furthermore, $\delta^{13}C$ was slightly higher at core BTGC8 (-20 ‰ to -21 ‰) compared with core BGGC5 (-21 ‰ to -22 ‰), the former is also showing slightly higher values of $\delta^{15}N$ from the deeper sections to the surface of the core (<7 ‰ to >10 ‰). This increase was less evident at core BGGC5, with values of ~9 ‰ at depths to >10 ‰ on the surface (Fig. 5a,b). The reduced TOC content was related to slightly higher $\delta^{13}C$ values (~ -20 ‰) in both cores.

4.3.3. Pollen record

Initial surveys at core BTGC8 (Tongoy Bay) revealed extremely low pollen abundances which hampered further palynology work. A comprehensive pollen analysis was only conducted for core BGGC5 (Guanaqueros Bay). The pollen record of core BGGC5 consisted of 29 samples shown in Figure 7. The record was divided into five general zones following visual observations of changes in the main pollen types and also assisted by CONISS cluster analysis.

Zone BG-1 (cal BP 8200 – 7600): This zone is dominated by the herbaceous taxa Chenopodiaceae, *Leucheria*-type, Asteraceae subfamily (subf.) Asteroideae, Apiaceae with overall high values for the wetland genus *Typha* spp.

Zone BG-2 (cal BP 7600 – 6500): This zone is also dominated by Chenopodiaceae, *Leucheria*-type and Asteraceae subf. Asteroideae. In addition, other non-arboreal elements such as *Ambrosia*-type, Poaceae, Brassicaceae and *Chorizanthe* spp. expand considerably.

Zone BG-3 (cal BP 6500 –3400): This zone is marked by a steady decline in Chenopodiaceae and *Leucheria*-type, and by the expansion of several other herbaceous elements, such as Euphorbiaceae, *Baccharis*-type and Brassicaceae.

Zone BG-4 (cal BP 3400 – 120): This zone is mostly dominated by Ast. subf. Asteroideae, and marked by the decline of Chenopodiaceae and *Leucheria*-type. Other coastal taxa –such as Euphorbiaceae, *Baccharis*-type, Asteraceae subf. Chichorioideae, *Quillaja saponaria*, Brassicaceae and *Salix* spp.– also expand in this zone.

Zone BG-5 (cal BP 120 – -60): The upper portion of the record is dominated by Asteraceae subf. Asteroideae and Poaceae, and marked by higher amounts of Geraniaceae, Asteraceae subf. Mutisieae, Myrtaceae and *Q. saponaria*. Additionally, this zone includes introduced pollen types such as *Rumex* spp. and *Pinus* spp. The latter is not shown in the diagram of Figure 8 because its abundance was minimal. Overall, the most distinctive trend revealed by core BGGC-5 is a long-term reduction in Chenopodiaceae and higher amounts of Euphorbiaceae and Asteraceae subf. Asteroideae. Along with these changes, a further expansion of several other pollen representative of the coastal shrub land vegetation began at about cal BP 6500.

4.4. Trace element distributions

Trace element distributions are shown in figures 8a and 8b for Guanaqueros (BGGC5) and Tongoy Bays (BTGC8), respectively. We use Al as a normalizing parameter for enrichment/depletion of elements due to its conservative behavior. The elements are presented as metal/Al ratios. Trace metals are sensitive to the presence of oxygen (U, Re, Mo) showing an increasing metal/Al ratio from the base of core BGGC5 (cal BP ~8210) up to cal BP 6500. After this peak, ratios showed a slight increase towards cal BP 1700, close to the beginning of the recent era, followed by a sharp reduction until present. Similarly, metal ratios at core BTGC8 increase over time, yet the peak was observed at cal BP ~1000. The exception to this trend was Mo, which reached a maximum value up to cal BP 6500 and then reduced steadily into the present. Additionally, metal/Al values were higher at core BGGC5. Iron revealed a clear upward trend around cal BP 3300 − 3500 at core BGGC5, which was not clearly observed at the Tongoy core. Instead, core BTGC8 showed peak Fe values around cal BP 6500 − 7800; in both cores, Fe increased in the past 130 years. No clear trend could be established for Mn.

A second group of elements (metal/Al ratios), including Ca, Ni, Cd and P (related to primary productivity and organic fluxes), showed a pattern similar to that of Mo/Al of core BGGC5, i.e. increasing values from cal BP ~8000 reaching highest values around cal BP 6500; after that the values followed constant reductions towards the present. A third group, consisting of Ba and Sr, exhibited a less clear pattern. Ca, Ni, Cd and P ratios at core BTGC8 showed only slightly decreasing values, and very low peak values compared to core BGGC5. Metal/Al ratios of Ba and Sr showed no substantial variation in time, except for Ca and Cd in the last 1000−1700 years. In general, all the elements' concentrations were lower and presented a long-term reduction pattern towards the present.

An exception to the previously described patterns was Cu/Al, which reach a maximum value at cal BP ~3600 ─3700 and showed a conspicuous upward trend in the past ~130 years. This was also observed at core BTGC8, but with lower concentrations than at core BGGC5.

The authigenic enrichment factor of elements was estimated according to: EF = $(Me/Al)_{sample}$ / $(Me/Al)_{detrital}$; where $(Me/Al)_{sample}$ is the bulk sample metal (Me) concentration normalized to Al content and the denomination "detrital" indicates a lithogenic background (Böning et al., 2009). Detrital ($[Me]_{detrital}$ and $[Al]_{detrital}$) concentrations were established considering local TM abundance, which is more accurate than using mean Earth crust values (Van der Weijden, 2002). We used average element concentrations on surface sediments (0−3 cm) of the Pachingo wetland (Table 3). The values suggest a large enrichment of nutrient-type elements in a period prior to cal BP 6500, following the trend of the Me/Al ratios, except for Ba and Fe which did not show authigenic enrichment. EFs showed a sharp enrichment reduction in recent times after cal BP 130 (Table 4).

5. Discussion

5.1. Sedimentary composition of the cores: terrestrial *versus* biogenic inputs

The sediments in the southern zones of the bays are a sink of fine particles transported from the north and the shelf (Fig. 5a, 5b), and respond to water circulation in the Guanaqueros and Coquimbo Bays (Fig. 1) having two counter-rotating gyres moving counterclockwise to the north and clockwise to the south (Valle-Levinson and Moraga, 2006) (Fig. 1). The differences established by the sediment composition of the bays shows that Guanaqueros Bay's sediments better represent the organic carbon flux to the bottoms, with higher accumulation rates (mean value: 16 g m^{-2} yr^{-1}) and higher amounts of siliceous microfossils. Furthermore, is it a better zone than Tongoy to identify pollen records (Figs. 5b, 6 and 7). Both areas have sediments composed by winnowed particles, relatively refractory material (C/N: 9─11), which has a slightly lower isotopic composition than the TOC composition in the column water (-18 ‰, Fig. 2), and transported by water circulating over the shelf.

The isotopic variations in $\delta^{13}C$ and $\delta^{15}N$ did not clearly establish differences between bays sediments, but minor differences in $\delta^{15}N$ would point to a greater influence of the upwelling's nutrient supply and the OMZ on the shelf, resulting in $\delta^{15}N$ of 9 – 10 ‰ in the Guanaqueros Bay, values which are slightly higher than in the Tongoy Bay sediments. This isotopic composition correspond to that of NO_3^- in upwelled waters (De Pol-Holz et al., 2007) in the range of those measured at northern and central Chile (~11 ‰; Hebbeln et al., 2000, De Pol-Holz et al., 2007), coming from the isotopic fractionation of NO_3^- during nitrate reduction within the OMZ, leaving a remnant NO_3^- enriched in ^{15}N (Sigman et al., 2009; Ganeshram et al., 2000 and references therein). At sediment core BTGC8, lower values (< 8 ‰) measured at greater depths within the core should account for the mix with isotopically lighter terrestrial organic matter (Sweeney and Kaplan, 1980) due to its vicinity to a small permanent wetland in the southern side of Tongoy Bay (Pachingo), the sediments of which have $\delta^{15}N$ of 1 – 8 ‰ (Muñoz et al., data will be published elsewhere), suggesting that Tongoy sediments contain a combination with continental material (Fig. 5b).

Thus, cores BGGC5 and BTGC8 in the Guanaqueros and Tongoy Bays are recording the variability of oceanographic conditions, but in the Tongoy core, the concentration of oceanographic proxies dilutes due to the input of terrigenous material. This helps to decipher the climatic variability considering that the main input of clastic material to the area takes place during major flooding events. Additionally, the main circulation of the bay system leads to favorable conditions for sedimentation and the preservation of organic marine proxies in the Guanaqueros Bay, hence making the sedimentary records of these sites complementary.

5.2. Temporal variability of primary productivity and the oxygenation of bottoms

Ca, Sr, Cd and Ni profiles suggest a lower share of organic deposition over time (Fig. 8a, 8b), consistent with the slight reduction of TOC content observed in the sediments (Figs. 5a, 5b), and concomitantly with other elements related to organic fluxes to the bottom and primary productivity. In the case of Ba, it is actively incorporated into phytoplankton biomass or adsorbed onto Fe oxyhydroxides, increasing the Ba flux towards the sediments. It is better preserved in less anoxic environments with moderate productivity (Torres et al., 1996; Dymond et al., 1992), as is the case of our study site (Gross Primary Productivity =0.35 to 2.9 g C $m^{-1}d^{-1}$; Daneri et al., 2000). The maximum Ba concentrations were before cal BP 6500. The same is true for Ca, Cd and Ni, suggesting that the maximum productivity and organic fluxes to the bottoms occurred during this period. After this age, the reduction in TOC and other nutrient-type elements (Ni, Sr, Ca, Cd) into the present is consistent with the rise in oxygen in bottoms. Hence, the slight rise of Ba from cal BP 4000 to the present (Fig. 8a) is a response to this less anoxic environment leading to negative correlation with TOC (-0.59; Table 5) due to Ba remobilization in anoxic conditions before cal BP 6500. On the other hand, P distribution showed a trend similar to that of TOC and other elements related to organic fluxes into the bottom (Ni, Cd), although with a lower correlation (~0.6). This is consistent with the distributions observed for U, Re, and Mo at core BGGC5, which indicate that anoxic or suboxic conditions were developed from cal BP 8200 to ~ cal BP 1700, but were stronger before cal BP 6500 (Fig. 8a, 8b). After this period and into the present, a remarkable reduction in their concentration suggests a more oxygenated bottom environment, concurrent with lower organic fluxes to the sediments. The Re profile shows the influence of suboxic waters not necessarily associated with higher organic matter fluxes to the bottom. Since this element is not scavenged by organic particles, its variability is directly related to oxygen changes (Calvert and Pedersen, 2007, and references therein). Additionally, it is strongly enriched above crustal abundance under suboxic conditions (Colodner et al., 1993; Crusius et al 1996), being >10 times at core BGGC5 (Table 4) before cal BP 1700. In the same manner, U shows a similar pattern and while organic deposition has an impact on its distribution (Zheng et al., 2002), it is also related to changes in bottom oxygen conditions.

Otherwise, the accumulation of P depends on the deposition rate of organic P (dead plankton, bones and fish scales) on the bottom, and is actively remineralized during aerobic or anaerobic bacterial activity. P and TOC showed a declining trend towards the present, suggesting reducing flux of organic matter over time, which was also observed for Ni and Cd distributions. Alternatively, reducing fluxes of organic proxies could be explained by the higher remineralization of organic material settled on the bottom due to higher oxygen availability, as shown by U, Mo and Re distributions (Figs. 8a, 8b). To better approach this issue, establishing the variability of primary productivity over time and the environmental factors that facilitate its development is required.

Productivity reconstructions were based on qualitative diatom and sponge spicules relative abundances, quantitative diatom counts (valves g^{-1}), and biogenic opal content only in core BGGC5, since core BTGC8 registered low valve counts (< 1 % in relative diatom abundance). However, in both cores diatom assemblages were represented mainly by *Ch.* resting spores, which are used as upwelling indicators (Abrantes 1988, Vargas et al., 2004). The downcore siliceous productivity based on opal distribution (Fig. 6) distinguished three main time intervals of higher productivity, which coincide with the ages highlighted by the distribution of the sedimentary proxies seen previously: (1) > cal BP 6500, (2) cal BP 1700 – cal BP 4500 and (3) recent times (CE 2015) – cal BP ~130. The opal accumulation rate in the first interval was remarkably high, amounting to ~27 ± 13 g m^2 yr^{-1} (range: 9 – 53 g $m^{-2}yr^{-1}$, Table 4), when *Chaetoceros* spores were predominant, indicating an upwelling intensification. During the first period, all metal proxies showed primary productivity increases before cal BP 6500, as indicated by opal accumulation within the sediments. Here, Cd and U accumulations in the sediments resulted in high Cd/U ratios, even at core BTGC8 (> 2; Fig. 6), pointing to very low oxygen conditions (Cd/U ratios could vary between 0.2 and 2 from suboxic to anoxic environment; Nameroff et al., 2002). In addition, during this period the presence of sulfidic conditions is suggested by Cd and Ni enrichments (>140 and 3, respectively, Table 4), since its buildup within the sediments is highly controlled by sulfide concentrations (Chaillou et al., 2002; Nameroff et al., 2002; Sundby et al., 2004), though Mo and Re where not especially high during this period (~17 and ~19, respectively, Table 4), all of which is suggesting an intensification of the upwelling during this time interval.

In the second interval, opal accumulation decreased to ~ 11 ± 4 g m^2 yr^{-1} (range: 2 – 21 g $m^{-2}yr^{-1}$, peaking at cal BP 3500–4000; Table 4, Fig. 6a), which is partially consistent with nutrient–type element distributions (Fig. 8a). Fe clearly shows higher values around cal BP 3500 (Fig. 8a), helping to boost primary productivity at this time, with a small diatom increase, measured as valves per gram and abundance (%) (Fig. 6a). Other elements showed less prominent accumulations (Ni, Cd, Ba, Ca and P), pointing to lower organic matter deposition into the sediments during this period (Fig. 8a). However, low oxygen conditions within the sediments are maintained, which could be more related to the manifestation of the oxygen minimum zone close to the coast, favoring Mo and Re accumulation until cal BP 1700 (Fig. 8a). Lower Cd/U ratios (~ 1; Fig. 6) were estimated, suggesting higher variations in primary productivity but with moderate changes in oxygen conditions at the bottoms. After cal BP 1700, there is an evident and remarkable reduction in organic fluxes to the sediments and a drastic change to a less reduced environment towards the present, suggesting a more oxygenated bottom environment concurrent with a reduction in primary productivity, except for the last ~130 years, when increasing opal accumulations and Cd/U ratios were estimated towards the present (mean opal value of 29 ± 14 g m^2 yr^{-1}, range: 3 – 40 g m^2 yr^{-1}; Fig. 5, 6, Table 4). However, low diatom abundances were observed (range: 0.5 – 4.9 x10^6 valves g^{-1}), probably because few sections of the core surface were analyzed for diatoms, leading to a low resolution of this measurement in the most recent period. In addition, the flux calculations were based on recent sedimentation rates, an estimation that tends to be higher than in the millennial time scale, overestimating the opal flux. In part, this explains the inconsistencies found between the rise in organic flux and low diatom abundance.

Otherwise, there is a conspicuous upward trend of Cu/Al, Fe/Al and Mn/Al in recent times, consistent with high organic fluxes to the bottoms (Fig. 5a,b; 8a,b) and concomitant with the decreasing trend and lower EFs of Re, U, and Mo (Fig. 8a, 8b, Table 4). This could be due to the presence of particulate forms and oxides formation (Peacock and Sherman, 2004; Vance et al., 2008; Little et al., 2014) occurring in the presence of an oxygenated environment that results in a high metal enrichment of these elements (EF_{cu}=4.6±0.5, Table 4). All of this is suggesting a higher productivity in the last 130 years occurring in a more oxygenated environment, which is actually contradictory. We assume that episodic oxygenation events related to El Niño change the original extent of these sensitive redox trace elements' accumulation because of their remobilization to soluble forms (Morford and Emerson, 1999); therefore, the increased frequency and intensity of El Niño would result in a mean effect which is observed as a gradual change in metal contents over time. Several observations made at the central Peruvian and south-central Chilean coasts (12 − 36 °S) reveal that present-day wet/dry variability associated with ENSO has a strong impact on the bottom ocean oxygenation (Escribano et al., 2004; Gutiérrez et al., 2008; Sellanes et al., 2007), suggesting a large increase in oxygen levels at bottoms during El Niño events that change the sediment geochemistry, the effects of which can be observed several months later. Thus, the oceanographic conditions that have prevailed in the past should be determinants not only for productivity but also for oxygen conditions above the bottoms, which is reflected in our sedimentary records.

5.3. Main climatic implications

According to modern climatology, paleoenvironmental records from semi-arid regions have been interpreted mainly based on the past variability in the intensity and latitudinal position of the SWW (Veit et al., 1996; Hebbeln et al., 2002; Lamy et al., 1999; Maldonado and Villagrán, 2002). This has an impact over relevant oceanographic characteristics such as upwelling and, therefore, productivity. We established marked differences in paleo productivity proxies and paleo-oxygenation in the last 8300 years (Figs. 6, 8); a high marine productivity prevailed during our first period (cal BP 8300 – 6500) according to what was established for central Chile between 10 and 5 kyr due to sustained mean La Niña-like conditions (De Pol-Holz et al., 2006; Kaiser et al., 2008), which is caused by reduced ENSO variability and a northward displacement of the ITCZ and implies more permanent southeast trades and hence, the upwelling of rich-nutrient cold waters (Koutavas et al., 2006). Our high productivities occurred concomitantly with low oxygen conditions at bottoms, both reaching a maximum level at cal BP 6500. This corresponds to the highest productive period in the last 8300 years, indicating an intensification of the SPSA and a weakening of SWW. In addition, our pollen records point to the main driest conditions during this period (Fig. 9), which matches with other reports in the area, indicating that an arid phase was developed until cal BP 5700 (Jenny et al 2002, Maldonado and Villagrán, 2006), and which could be extended until cal BP 4200 (Maldonado and Rozas, 2008; Maldonado and Villagrán, 2002, 2006). This period was characterized by reduced rainfalls and intense coastal humidity, which have been associated to coastal fogs that frequently occur during the spring due to a strengthening of the SPSA (Vargas et al., 2006; Garreaud et al 2008; Ortega et al., 2012) and La Niña–like conditions, associated with the cold phase of the Pacific Decadal Oscillation, which explains the main variability of the SPSA (Ancapichún and Garcés-Vargas, 2015). Strengthened easterlies favor upwelling and cause SST cooling, also pointing to a northward location of the ITCZ which was suggested for the early-mid Holocene (Kaiser et al., 2008; Lamy et al., 2010). This would be consistent with our records and points to more favorable conditions for upwelling strengthening around cal BP 6500 at central Chile. However, others have suggested a reduced ENSO variance in this period (Rein et al., 2005) linked to fresh water melting that counteracted the insolation regime (Braconnot et al., 2012), but points to a more limited cold-dry period between 6700 – 7500 years ago. This could be due to less frequent or less intense warm anomalies related to a CP mode ENSO, which produce moderate El Niño events at the Central Pacific (CP) and strong La Niña off Peru (Carré et al., 2014), matching our records of maximum productivity.

After this date, a decreasing productivity occurred under more warm and humid climatic conditions that would be due to an enhancement of regional precipitation in the northern margin of SWW (Jenny et al., 2003; Maldonado and Villagrán, 2006), consistent with the gradual rise of K/Ca, Fe, Al and Pb distributions in our cores (Fig. 8, 9), usually considered to be indicators of continental input by fluvial or aerial transport (Calvert and Pedersen, 2007; Kaiser et al., 2008; Govin et al., 2012; Ohnemus and Lam, 2015; Saito et al., 1992; Xu et al., 2015). This would contradict a second period of reduced (or weak) ENSO activity reported for cal BP 4500, and also with others who sustain that this weak activity condition took place from cal BP 6000 to 4000 (Koutavas and Joanides, 2012; Carré et al., 2014). It is also consistent with the pollen records of central Chile that suggest an arid phase from cal BP 6200 until cal BP 4200 (Maldonado and Villagrán, 2006). No sharply contrasting dry and cold periods were identified after cal BP 6500, mostly a gradual increase in humidity and a weakening in paleo-productivity proxies (Fig. 8, 9) that would be consistent with the beginning of higher ENSO variability for central Chile after cal BP 5700 (Jenny et al., 2002, Maldonado and Villagrán, 2002, 2006). Nonetheless, the slight rise of diatom abundance and opal concentrations between cal BP 4500 and 3000, along with a slight accumulation of nutrient elements (Ni, Cd, Fe and Ca concentrations; Fig. 8) and small rises in organic carbon flux and Cd/U ratios (Fig. 5, 6), would be related to an increase in continental nutrient inputs that help primary productivity development observed in sedimentary records for the north-central Chilean margin (Dezileau et al., 2004; Kaiser et al., 2008). A peak of La Niña activity around cal BP 3000‒4000 has been otherwise proposed for the tropical east Pacific (Toth et al., 2012), which would also explain the increase in the productivity's proxies. This is a period of increased ENSO variability from cal BP~ 5700, and stronger El Niño events after cal BP 4000‒4500, concomitant with the high variability of latitudinal displacements of the ITCZ related to the seasonality of insolation described for the mid and late Holecene period (Haug et al., 2001; Toth et al., 2012; Carré et al., 2014). This is consistent with the occurrence of alluvial episodes in the area caused by more frequent or heavier rainfall events over time, related to intensified Westerlies and increased El Niño events (Jenny et al., 2002; 2003; Ortega et al., 2012; Ortega et al., 2019). This is leading to more humid conditions and greater continental inputs as suggested by our pollen moisture index and sedimentary records. In spite of the dominance of warm events described for this period, they were not strong enough to change the suboxic conditions at the bottoms, which were maintained until cal BP 1700 (Fig. 8; see U, Mo and Re). After that, the drastic oxygenation of the bottoms occur during higher frequency and intensity of flooding events recorded in central Chile in the last 2000 years, consistent with more frequent El Niño events (Jenny et al., 2002, Toht et al., 2012). In this regard, oxygen variations at the bottoms would be related to less intense OMZs during warm El Niño-like phases (and vice versa during La Niña). These tend to be associated with low productivity (Salvatteci et al., 2014), and, in turn, reduce organic fluxes and oxygen consumption during organic matter diagenesis. Thus, more frequent El Niño events in recent times could be the cause for oxygen increments and lower productivity, which has been deduced from very low chlorins (or photosynthetic pigments) sediment records in the past 2000 years (Rein, 2007), which is consistent with our observations.

In recent times, the most extreme and longer ENSO events have been established in the 20th century, mostly after the 1940s and characterized by severe floods and droughts linked to global climate change (Gergis and Fowler, 2009). Similarly, warmer periods have been characterized by lower primary productivity and more oxygenated waters over the shelf. However, enhanced solar heat over the land in northern Chile results in the intensification of coastal southerly winds, strengthening upwelling during warmer ENSO periods (Vargas et al., 2007). If this is coming along with Fe inputs to the bay system, it could explain the productivity records during recent times. In addition, during the El Niño conditions, the normal dominance of diatoms is replaced by smaller size phytoplankton, making a relevant contribution to overall primary production (Iriarte et al., 2000; Rutlland and Montecino, 2002; Iriarte and Gozalez, 2004; Escribano et al., 2004) that would change sedimentary diatom records but maintaining organic fluxes to the bottoms.

6. Conclusions

The ocean circulation in our study sites seems to impact both places differently, leaving more variable grain compositions and higher TOC contents in the Guanaqueros Bay (core BGGC5) than in the Tongoy Bay (core BTGC8), with the latter increasingly impacted by terrigenous inputs due to the flow of several creeks during major flooding events. Nevertheless, both core records sustain a reduction of organic flux to the bottoms after cal BP ~6500 and into present times. This is probably due to higher ENSO variability over time, sustained by an increase in the pollen moisture index, suggesting a long-term rise in precipitation after cal BP 6500. At such point, an overall expansion of the coastal vegetation and larger river runoffs occurred, expanding the grain size of the sediments and increasing the concentrations of elements with an important continental source (Al, Fe, K and Pb). Therefore, eolian and fluvial transportation seems to become relevant after this date to boost phytoplankton when ENSO variability increases and in the face of stronger El Niño events.

Our results suggest that the geochemistry and sedimentary properties of coastal shelf environments in north-central Chile have changed considerably during the Holocene period, suggesting two relevant changes in redox conditions and productivity, pointing to a more reducing environment and higher productivity around cal BP 6500. After that, a less reducing environment along with decreasing trends in primary productivity and increased humid conditions in time, were developed until cal BP 1700. The northward shifts of the Southern Westerly Wind belt, in addition to an increased frequency of El Niño events, have been proposed as the main drivers for climatic conditions during this period. These elements have introduced a high variability in primary productivity during this time interval. Additionally, this also impacted the accumulation of organic matter due to an intensification of its remineralization, showing a decreasing trend in the buildup of nutrient type elements and organic carbon burial rates towards the present. The decrease in oxygen content at bottoms was highly influenced during El Niño events, something that seems to have been operating at higher frequencies after cal BP 1700, and especially after cal BP 130, when the most extreme events become more frequent.

Finally, these changes highlight the sensitivity of these environments to climate variability at different timescales, which is consistent with the description of past regional climatic trends. Based on the dramatic changes observed in the last 1700 years, future changes are expected in the ongoing scenario of global warming at unprecedented rates.

7. References

Abrantes, F.: Diatom assemblages as upwelling indicators in surface sediments off Portugal, Mar. Geol., 85(1), 15–39, doi:10.1016/0025-3227(88)90082-5, 1988.

Ancapichún, S. and Garcés-Vargas, J.: Variability of the Southeast Pacific Subtropical Anticyclone and its impact on sea surface temperature off north-central Chile Variabilidad del Anticiclón Subtropical del Pacífico Sudeste y su impacto sobre la temperatura superficial del mar frente a la costa centro-norte de Chile, Cienc. Mar., 41(1), 1–20, doi:10.7773/cm.v41i1.2338, 2015.

Appleby, P. G. and Oldfield, F.: The calculation of lead-210 dates assuming a constant rate of supply of unsupported210Pb to the sediment, Catena, 5(1), 1–8, doi:10.1016/S0341-8162(78)80002-2, 1978.

Bevington, P. and Robinson, K. (Eds.): Error analysis. In: Data Reduction and Error Analysis for the Physical Sciences, WCB/McGraw-Hill, USA, 38–52, 1992

Blanco, J.L., Carr, M-E., Thomas, A.C. and Strub, T.: Hydrographic conditions off northern Chile during the 1996–1998 La Niña and El Niño events, J. Geophys. Res., 107, C3, 3017, 10.1029/2001JC001002, 2002.

Blott, S. J. and Pye, K.: Gradistat: A Grain Size Distribution and Statistics Package for the Analysis of Unconcolidated Sediments, Earth Surf. Process. Landforms, 26, 1237–1248, doi:10.1002/esp.261, 2001.

Böning, P., Brumsack, H.-J., Schnetger, B. and Grunwald, M.: Trace element signatures of Chilean upwelling sediments at 36°S. Mar. Geol., 259, 112–121, 2009.

Braconnot, P., Luan, Y., Brewer, S. and Zheng, W.: Impact of Earth's orbit and freshwater fluxes on Holocene climate mean seasonal cycle and ENSO characteristics. Clim. Dyn., 38, 1081–1092, doi: 10.1007/s00382-011-1029-x, 2012.

Calvert, S. E. and Pedersen, T. F.: Chapter Fourteen Elemental Proxies for Palaeoclimatic and Palaeoceanographic Variability in Marine Sediments: Interpretation and Application, Dev. Mar. Geol., 1(7), 567–644, doi:10.1016/S1572-5480(07)01019-6, 2007.

Carré, M., Sachs, J.P., Purca, S., Schauer, A.J. and Braconnot, P., Falcón, R.A., Julien, M., Lavallée, D.: Holocene history of ENSO variance and asymmetry in the eastern tropical Pacific, Science 345, 1045‒1048. DOI: 10.1126/science.1255768. 2014.

Carré, M., Jackson, D., Maldonado, A., Chase, B.M. and Sachs, J.P.: Variability of 14C reservoir age and air–sea flux of CO2 in the Peru–Chile upwelling region during the past 12,000 years, Quat. Res., 85, 87–93, 2016.

Chaillou, G., Anschutz, P., Lavaux, G., Schäfer, J. and Blanc, G.: The distribution of Mo, U, and Cd in relation to major redox species in muddy sediments of the Bay of Biscay, Mar. Chem., 80(1), 41–59, doi:10.1016/S0304-4203(02)00097-X, 2002.

Colodner, D., Sachs, J., Ravizza, G., Turekian, K. K. and Boyle, E.: The geochemical cycle of Re: a reconnaissance, Earth Planet. Sci. Lett., 117, 205–221, doi:10.1016/0012-821X(93)90127-U, 1993.

Croquette, M., Eldin, G., Grados, C. and Tamayo, M.: On differences in satellite winds product and their effects in estimating coastal upwelling processes in the South-east Pacific, Geophys. Res. Lett., 34 L11 608, doi: 10.1029/2006GL027538. 2007.

Crusius, J., Calvert, S., Pedersen, T. and Sage, D.: Rhenium and molybdenum enrichments in sediments as indicators of oxic, suboxic and sulfidic conditions of deposition, Earth Planet. Sci. Lett., 145(1–4), 65–78, doi:10.1016/S0012-821X(96)00204-X, 1996.

Daneri, G., Dellarossa, V., Quiñones, R., Jacob, B., Montero, P. and Ulloa, O.: Primary production and community respiration in the Humboldt Current System off Chile and associated oceanic areas, Mar. Ecol. Prog. Ser., 197, 41–49, doi:10.3354/meps197041, 2000.

De Pol-Holz, R., Ulloa, O., Lamy, F., Dezileau, L., Sabatier, P., and Hebbeln, D.: Late Quaternary variability of sedimentary nitrogen isotopes in the eastern South Pacific Ocean, Paleoceanography, 22, PA2207, doi: 10.1029/2006 PA001308, 2007.

Dezileau, L., Ulloa, O., Hebbeln, D., Lamy, F., Reyss, J. L. and Fontugne, M.: Iron control of past productivity in the coastal upwelling system off the Atacama Desert, Chile, Paleoceanography, 19(3), doi:10.1029/2004PA001006, 2004.

Dymond, J., Suess, E. and Lyle, M.: Barium in deep- sea sediment: A geochemical proxy for paleoproductivity, Paleoceanography, 7(2), 163–181, 1992.

Escribano, R., Daneri, G., Farías, L., Gallardo, V. A., González, H. E., Gutiérrez, D., Lange, C. B., Morales, C. E., Pizarro, O., Ulloa, O. and Braun, M.: Biological and chemical consequences of the 1997-1998 El Niño in the Chilean coastal upwelling system: A synthesis, Deep. Res. Part II Top. Stud. Oceanogr., 51(20–21), 2389–2411, doi:10.1016/j.dsr2.2004.08.011, 2004.

Faegri, K. and Iversen, J.: Textbook of pollen analysis, IV. The Blackburn Press, New Yersey, 328 pp., 1989.

Figueroa, D. and Moffat, D.: On the influence of topography in the induction of coastal upwelling along the Chilean coast Geophys. Res. Lett. 27, 3905-3908, 2000.

Flynn, W. W.: The determination of low levels of polonium-210 in environmental materials, Anal. Chim. Acta, 43, 221–227, 1968.

Gallardo, M.A., González, A., Ramos, M., Mujica, A., Muñoz, P., Sellanes, J. and Yannicelli, B.: Reproductive patterns in demersal crustaceans from the upper boundary of the OMZ off north-central Chile, Cont. Shelf. Res. 141, 26–37, 2017.

Ganeshram, R.S., Pedersen, T. F., Calvert, S.G., McNeill, G. and Fontugne, M.: Glacial-interglacial variability in denitrification in the world's oceans: Causes and consequences. Paleoceanography, 15(4), 361– 376, 2000.

Garreaud, R., Barichivich, J., Christie, D. and Maldonado, A.: Interanual variability of the coastal fog at Fray Jorge relict forest in semiarid Chile. Journal of Geophysical Research. Vol 113. G04011, doi:10.1029/2008JG000709. 2008.

Garreaud, R., Vuille. M., Compagnuccic, R. and Marengo, J.: Present-day South American climate, Palaeogeogr. Palaeocl., 281, 180-195, doi:10.1016/j.palaeo.2007.10.032, 2009

Gergis, J.L. and Fowler, A.M.: A history of ENSO events since A.D. 1525: implications for future clim. change. Climatic Change, 92,343–387, doi: 10.1007/s10584-008-9476-z, 2009.

Govin, A., Holzwarth, U., Heslop, D., Ford Keeling, L., Zabel, M., Mulitza, S., Collins, J. A. and Chiessi, C. M.: Distribution of major elements in Atlantic surface sediments (36°N-49°S): Imprint of terrigenous input and continental weathering, Geochemistry, Geophys. Geosystems, 13(1), 1–23, doi:10.1029/2011GC003785, 2012.

Grimm, E.: CONISS: a fortran 77 program for stratigraphically constrained cluster analysis by the method of incremental sum of squares. Computers and Geociences 13–35, 1987.

Gutiérrez, D., Sifedine, A., Reyss, J.L., Vargas, G., Velazco, F., Salvattci, R., Ferreira, V., Ortlieb, L., Field, D., Baumgartner, T., Boussafir, M., Boucher, H., Valdés, J., Marinovic, L., Soler, P. and Tapia, P: Anoxic sediments off Central Peru record interannual to multidecadal changes of climate and upwelling ecosystem during the last two centuries, Adv. Geosci. 6, 119–125, 2006.

Gutiérrez, D., Enríquez, E., Purca, S., Quipuzcoa, L., Marquina, R., Flores, G. and Graco, M.: Oxygenation episodes on the continental shelf of central Peru: Remote forcing and benthic ecosystem response. Prog. Oceanogr., 79, 177–189, 2008.

Hansen, H. P. and Koroleff, F.: Determination of nutrients. In Methods of Seawater Analysis. Grasshoff, K., Kremling, K. and Ehrhardt, M. (Eds.), Wiley-VCH Verlag GmbH, Weinheim, Germany, 159–228, 1999.

Haug, G.H., Hughen, K.A., Sigman, D.M., Peterson, L.C. and Röhl, U.: Southward Migration of the Intertropical Convergence Zone through the Holocene. Sci. 293, 1304–1307, 2001.

Hebbeln, D., Marchant, M., Freudenthal, T. and Wefer, G.: Surface distribution along the Chilean continental slope related to upwelling and productivity. Mar. Geol., 164, 119–137, 2000.

Hebbeln, D., Marchant, M. and Wefer, G.: Paleoproductivity in the southern Peru ^ Chile Current through the last 33 000 yr, Mar. Geol., 186, 2002.

Helly, J. and Levin. L.: Global distribution of naturally occurring marine hypoxia on continental margin, Deep-Sea Res. Pt. I, 51, 1159-1168, 2004.

Heusser, C. J. and Moar, N. T.: Pollen and spores of chile: Modern types of the pteridophyta, gymnospermae, and angiospermae, New Zeal. J. Bot., 11(2), 389–391, doi:10.1080/0028825X.1973.10430287, 1973.

Iriarte, J.L., Pizarro, V.A., Troncoso, V.A. and Sobarzo, M.: Primary production and biomass of size-fractionated phytoplankton off Antofagasta, Chile 23–24°S during pre-El Niño and El Niño 1997, J. Marine Syst., 26, 37–51, 2000.

Iriarte, J.L. and González, H.: Phytoplankton size structure during and after the 1997/98 El Niño in a coastal upwelling area of the northern Humboldt Current System, Mar. Ecol. Prog. Ser., 269, 83 – 90, 2004.

Jenny, B., Valero-Garcés, B.L., Urrutia, R., Kelts, K., Veit, H., Appleby, P.G., Geyh, M.: Moisture changes and fluctuations of the Westerlies in Mediterranean Central Chile during the last 2000 years:The Laguna Aculeo record (33°50°S, Quat. Int. 87, 3–18, 2002.

Jenny, B., Wilhelm, D. and Valero-Garcés, B.L.: The Southern Westerlies in Central Chile: Holocene precipitation estimates based on a water balance model for Laguna Aculeo (33°50’S), Clim. Dynam., 20, 269–280, DOI 10.1007/s00382-002-0267-3, 2003.

Kaiser, J., Schefuß, E., Lamy, F., Mohtadi, M. and Hebbeln, D.:Glacial to Holocene changes in sea surface temperature and coastal vegetation in north central Chile: high versus low latitude forcing, Quat. Sci. Rev., 27, 2064–2075, 2008.

Koutavas, A. and Joanides, S.: El Niño–Southern Oscillation extrema in the Holocene and Last Glacial Maximum, Paleoceanography, 27, PA4208, doi:10.1029/2012PA002378, 2012.

Koutavas, A., deMenocal, P.B., Olive, G.C. and Lynch-Stieglitz, J.: Mid-Holocene El Niño–Southern Oscillation (ENSO) attenuation revealed by individual foraminifera in eastern tropical Pacific sediments, 34(12), 993–996, doi: 10.1130/G22810A, 2006.

Lamy F., Hebbeln, D.and Wefer, G.: High-Resolution Marine Record of Climatic Change in Mid-latitude Chile during the Last 28,000 Years Based on Terrigenous Sediment Parameters, Quat. Res., 51, 83–93, 1999.

Lamy, F., Kilian, R., Arz, H.W., Francois J-P., Kaiser, J.,Prange, M. and Steinke, T.: Holocene changes in the position and intensity of the southern westerly wind belt, Nat. Geosci., 3, 695–699, 2010.

Little, S. H., Vance, D., Walker-Brown, C. and Landing, W. M.: The oceanic mass balance of copper and zinc isotopes, investigated by analysis of their inputs, and outputs to ferromanganese oxide sediments, Geochim. Cosmochim. Acta, 125, 673–693, doi:10.1016/j.gca.2013.07.046, 2014.

Maldonado, A. and Rozas, E.: Clima y Paleoambientes durante el Cuaternario Tardío en la Región de Atacama, in Libro Rojo de la Flora Nativa y de los Sitios Prioritarios para su Conservación: Región de Atacama, pp. 293–304., 2008.

Maldonado, A. and Villagrán, C.,: Paleoenvironmental changes in the semiarid coast of Chile (~32°S) during the last 6200 cal years inferred from a swamp-forest pollen record. Quat. Res., 58, 130–138, 2002.

Maldonado, A. and Villagrán, C.: Climate variability over the last 9900 cal yr BP from a swamp forest pollen record along the semiarid coast of Chile, Quat. Res., 66(2), 246–258, doi:10.1016/j.yqres.2006.04.003, 2006.

Mazzullo, J., Leschak, P. and Prusak, D.: Sources and distribution of late Quaternary silt in the surficial sediment of the northeastern continental shelf of the United States. Mar. Geol., 78:241 254, 1988.

McManus, J., Berelson, W. M., Severmann, S., Poulson, R. L., Hammond, D. E., Klinkhammer, G. P., and Holm, C.: Molybdenum and uranium geochemistry in continental margin sediments: Paleoproxy potential, Geochim. Cosmochim. Acta, 70, 4643–4662, 2006.

Merino-Campos, V., De Pol-Holz, R. Southon, J., Latorre, C., Collado-Fabbri, S.: Marine radiocarbon reservoir age along the Chilean continental margin, Radiocarbon, 81, 1–16, doi:10.1017/RDC.2018.81, 2018.

Montecinos, A., and Aceituno, P.: Seasonality of the ENSO-Related Rainfall Variability in Central Chile and Associated Circulation Anomalies. J. Climate., 16, 281–296, 2003.

Montecinos, S., Gutiérrez, J. R., López-Cortés, F. and López, D.: Climatic characteristics of the semi-arid Coquimbo Region in Chile, J. Arid Environ., 126, 7–11, doi:10.1016/j.jaridenv.2015.09.018, 2016.

Moraga-Opazo, J., Valle-Levinson, A., Ramos, M. and Pizarro-Koch, M.: Upwelling-Triggered near-geostrophic recirculation in an equatorward facing embayment, Cont. Shelf Res., 31, 1991–1999, 2011.

Morford, J. and Emerson, S.: The geochemistry of redox sensitive trace metals in sediments, Geochim. et Cosmochim. Acta, 63, 11/12, 1735–1750, 1999.

Mortlock, R. A. and Froelich, P. N.: A simple method for the rapid determination of biogenic opal in pelagic marine sediments, Deep Sea Res. Part A, Oceanogr. Res. Pap., 36(9), 1415–1426, doi:10.1016/0198-0149(89)90092-7, 1989.

Nameroff, T., Balistrieri, L. and Murray, W.: Suboxic trace metals geochemistry in the eastern tropical North Pacific, Geochim Cosmochim Ac., 66(7), 1139–1158, 2002.

Ohnemus, D. C. and Lam, P. J.: Cycling of lithogenic marine particles in the US GEOTRACES North Atlantic transect, Deep. Res. Part II Top. Stud. Oceanogr., 116, 283–302, doi:10.1016/j.dsr2.2014.11.019, 2015.

Ortega, C., Vargas, G., Rutllant, J.A., Jackson, D. and Méndez, C.: Major hydrological regime change along the semiarid western coast of South America during the early Holocene, Quaternary Res., 78, 513-527, 2012.

Ortega, C., Vargas, G., Rojas, M., Rutllant, J.A., Muñoz, P., Lange, C.B., Pantoja, S., Dezileau, L. and Ortlieb, L.: Extreme ENSO-driven torrential rainfalls at the southern edge of the Atacama Desert during the late Holocene and their projection into the 21th century, GloPlaCha, 175, 226 – 237, https://doi.org/ 10.1016/j.gloplacha.2019.02.011, 2019.

Paytan, A.: Ocean paleoproductivity, Encyclopedia of Paleoclimatology and Ancient Environments, Encyclopedia of Earth Science Series, Gornitz, V. (Ed.), Kluwer Academic Publishers. 2008.

Peacock, C.L. and Sherman, D.M.: Copper(II) sorption onto goethite, hematite and lepidocrocite: a surface complexation model based on ab initio molecular geometries and EXAFS spectroscopy. Geochim. Cosmochim. Ac., 68, 2623–2637, 2004.

Pizarro, O., Hormazabal, S., Gonzalez, A. and Yañez, E.: Variabilidad del viento, nivel del mar y temperatura en la costa norte de Chile, Invest. Mar., 22, 85–101, 1994.

Pizarro, O., Shaffer, G., Dewitte, B. and Ramos, M.: Dynamics of seasonal and interannual variability of the Peru-Chile Undercurrent, Geophys. Res. Lett., 29(12), 28–31, doi:10.1029/2002GL014790, 2002.

Quintana, J.M. and Aceituno, P.: Changes in the rainfall regime along the extratropical west coast of South America (Chile): 30-43º S, Atmosfera, 25(1), 1 – 22, 2012.

Ramos, M., Pizarro,O., Bravo, L. and Dewitte, B.: Seasonal variability of the permanent thermocline off northern Chile, Geophys. Res. Lett., 33, L09608, doi:10.1029/2006GL025882, 2006.

Ramos, M., Dewitte, B., Pizarro, O. and Garric, G.: Vertical propagation of extratropical Rossby waves during the 1997–1998 El Niño off the west coast of South America in a medium-resolution OGCM simulation, J. Geophys. Res., 113, C08041, doi:10.1029/2007JC004681, 2008.

Rahn, D.A. and Garreaud, R.A.: A synoptic climatology of the near-surface wind along the west coast of South America. Int. J. Climatol., 34(3), 780–792, doi: 10.1002/joc.3724, 2013.

Reimer, P. J., Bard, E., Bayliss, A., Beck, J. W., Blackwell, P. G., Ramsey, C. B., Buck, C. E., Cheng, H., Edwards, R. L., Friedrich, M., Grootes, P. M., Guilderson, T. P., Haflidason, H., Hajdas, I., Hatté, C., Heaton, T. J., Hoffmann, D. L., Hogg, A. G., Hughen, K. A., Kaiser, K. F., Kromer, B., Manning, S. W., Niu, M., Reimer, R. W., Richards, D. A., Scott, E. M., Southon, J. R., Staff, R. A., Turney, C. S. M. and van der Plicht, J.: IntCal13 and Marine13 Radiocarbon Age Calibration Curves 0–50,000 Years cal BP, Radiocarbon, 55(4), 1869–1887, doi:10.2458/azu_js_rc.55.16947, 2013.

Rein, B., Lückge, A., Reinhardt, L., Sirocko, F., Wolf, A. and Dullo, W-C.: El Niño variability off Peru during the last 20,000 years, Paleoceanogr., PA4003, doi:10.1029/2004PA001099, 2005

Rein, B.: How do the 1982/83 and 1997/98 El Niños rank in a geological record from Peru?, Quat. Int., 161, 56–66, 2007.

Rutlland, J. and Fuenzalida, H.: Synoptic aspects of the central Chile Rainfall variability associated with the southern oscillation, Int. J. Climatol., 11, 63 – 76, 1991.

Rutlland, J. and Montecino, V.: Multiscale upwelling forcing cycles and biological response off northcentral Chile, Rev. Chil. Hist. Nat., 7, 217-231, 2002

Sabatier, P., Dezileau, L., Blanchemanche, P., Siani, G., Condomines, M., Bentaleb, I. and Piquès, G.: Holocene variations of radiocarbon reservoir ages in a mediterranean lagoonal system, Radiocarbon, 52(1), 91–102, doi:10.1017/S0033822200045057, 2010.

Saito, C., Noriki, S. and Tsunogai, S.: Particulate flux of Ai, a component of land origin, in the western North Pacific, Deep-Sea Res., 39, 1315–1327, 1992.

Salvatteci, R., Gutiérrez, D., Field, D., Sifeddine, A., Ortlieb, L., Bouloubassi, I., Boussafir, M., Boucher, H. and Cetin, F.: The response of the Peruvian Upwelling Ecosystem to centennial-scale global change during the last two millennia, Clim. Past, 10(2), 715–731, doi:10.5194/cp-10-715-2014, 2014.

Schrader H. J. and Gersonde, R.: Diatoms and silicoflagellates. Utrecht Micropaleontol. Bull. 17, 129–176, 1978.

Sellanes, J., Quiroga, E., Neira, C., Gutiérrez, D.: Changes of macrobenthos composition under different ENSO cycle conditions on the continental shelf off central Chile, Cont. Shelf. Res. 27, 1002 –1016, 2007.

Shaffer, G., Pizarro, O. Djurfeldt, L., Salinas, S. and Rutllant, J.: Circulation and low-frequency variability near the Chilean coast: Remotely forced fluctuations during the 1991– 92 El Niño, J. Phys. Oceanogr., 27, 217– 235, 1997.

Shaffer, G., Hormazabal, S., Pizarro, O. and S. Salinas.: Seasonal and interannual variability of currents and temperature over the slope of central Chile. J. Geophys. Res., 104, C12, 29,951-29,961, 1999.

Siebert, C., Nägler, T.F., von Blackenburg, F. and Kramers, J.D.: Molybdenum isotope records as a potential new proxy for paleoceanography. Earth Planet. Sci. Lett., 6643, 1–13, 2003.

Sigman, D.M., Karsh, K.L. and Casciotti, K.L.: Ocean process tracers: nitrogen isotopes in the ocean. Encyclopedia of ocean science, 2nd edn Elsevier, Amsterdam, 2009.

Sundby, B., Martinez, P. and Gobeil, C.: Comparative geochemistry of cadmium, rhenium, uranium, and molybdenum in continental margin sediments, Geochim. Cosmochim. Ac., 68, 2485–2493, 2004.

Sweeney, R. E. and Kaplan I. R.: Natural abundances of 15N as a source indicator of nearshore marine sedimentary and dissolved nitrogen, Mar. Chem., 9, 81–94, 1980.

Thiel, M., Macaya, E.C., Acuña, E., Artnz, W.F., Bastias. H., Brokordt. K., Camus, P.A., Castilla, J.C., Castro, L.R., Cortés, M., Dumont, C.P., Escribano, R., Fernandez, M., Gajardo, J.A., Gaymer, C.F., Gómez, I., González, A.E., González, H.E., Haye, P., Illanes, J.E., Iriarte, J.L., Lancellotti, D.A., Luna-Jorquera, G., Luxoro, C., Manriquez, P.H., Marín, V., Muñoz, P., Navarrete, S.A., Pérez, E., Poulin, E., Sellanes, J., Sepúlveda, H.H., Stotz, W., Tala, F., Thomas, A., Vargas, C.A., Vásquez, J.A., Vega, J.M.: The Humboldt Current system of Northern and Central Chile: Oceanographic processes, ecological interactions and socioeconomic feedback. Oceanogr. Mar. Biol. An Annual Review, 45, 195–344, 2007.

Torres, M. E., Brumsack, H. J., Bohrman, G. and Emeis, K. C.: Barite front in continental margin sediments: a new look at barium remobilization in the zone of sulfate reduction and formation of heavy barites in diagenetic fronts, Chem. Geol., 127, 125–139, 1996.

Torres, R., and Ampuero, P.: Strong CO2 outgassing from high nutrient low chlorophyll coastal waters off central Chile (30°S): The role of dissolved iron, Estuar. Coast. Shelf S., 83, 126–132, doi:10.1016/j.ecss.2009.02.030, 2009.

Toth, L.T., Aronson, R.B., Vollmer, S.V., Hobbs, J.W., Urrego, D.H., Cheng, H., Enochs, I.C., Combosch, D.J., van Woesik, R., Macintyre, J.G.: ENSO Drove 2500-Year Collapse of Eastern Pacific Coral Reefs, Science 337, 81– 84, doi: 10.1126/science.1221168 2012

Tribovillard, N., Algeo, T. J., Lyons, T. and Riboulleau, A.: Trace metals as paleoredox and paleoproductivity proxies: an update. Chem. Geol., 232, 12–32, 2006.

Ulloa, O., Escribano, R., Hormazabal, S., Quiñones, R.A., Gonzalez, R., Ramos, M.,: Evolution and biological effects of the 1997-98 E1 Niño in the upwelling ecosystem off northern Chile, Geophys. Res. Lett., 28, 1591– 1594, 2001.

Ulloa, O., Canfield, D.E., DeLong, E.F., Letelier, R.L. and Stewart, F.J.: Microbial oceanography of anoxic oxygen minimum zones. PNAS, 109, 15996–16003, doi/10.1073/pnas.1205009109, 2012.

Vance, D., Archer, C., Bermin, J., Perkins, J., Statham, P. J., Lohan, M. C., Ellwood, M. J. and Mills, R. A.: The copper isotope geochemistry of rivers and the oceans, Earth Planet. Sc. Lett., 274, 204–213, 2008.

Valle-Levinson, A., Moraga, J., Olivares, J. and Blanco, J. L.: Tidal and residual circulation in a semi-arid bay: Coquimbo Bay, Chile. Cont. Shelf Res., 20, 2009–2018, 2000.

Valle-Levinson, A. and Moraga-Opazo, J.: Observations of bipolar residual circulation in two equatorward-facing semiarid bays, Cont. Shelf Res., 26(2), 179–193, doi:10.1016/j.csr.2005.10.002, 2006.

Van der Weijden, C.: Pitfalls of normalization of marine geochemical data using a common divisor, Mar. Geol., 184, 167–187, 2002.

Vargas, G., Ortlieb, L., Pichon, J. J., Bertaux, J. and Pujos, M.: Sedimentary facies and high resolution primary production inferences from laminated diatomacous sediments off northern Chile (23°S), Mar. Geol., 211(1–2), 79–99, doi:10.1016/j.margeo.2004.05.032, 2004.

Vargas, G., Rutllant, J., Ortlieb, L.: ENSO tropical–extratropical climate teleconnections and mechanisms for Holocene debris flows along the hyperarid coast of western South America (17°–24°S), Earth Planet. Sci. Lett., 249, 467–483, 2006.

Vargas, G., Pantoja, S., Rutllant, J., Lange, C. and Ortlieb, L.: Enhancement of coastal upwelling and interdecadal ENSO-like variability in the Peru-Chile Current since late 19th century. Geophys. Res. Lett., 34, L13607, 2007.

Veit, H.: Southern Westerlies during the Holocene deduced from geomorphological and pedological studies in the Norte Chico, Northern Chile (27–33°S). Palaeogeogr., Palaeoclimatol., Palaeoecol., 123, 107–119, 1996.

Xu, G., Liu, J., Pei, S., Kong, X., Hu, G. and Gao, M.: Source identification of aluminum in surface sediments of the Yellow Sea off the Shandong Peninsula, Acta Oceanol. Sin., 34(12), 147–153, doi:10.1007/s13131-015-0766-9, 2015.

Zheng, Y., Anderson, R. F., van Geen, A. and Fleisheir, M.Q.: Preservation of non-lithogenic particulate uranium in marine sediments. Geochim. Cosmochim. Ac., 66, 3085–3092, 2002.

Acknowledgments

We would like to thank the R/V Stella Maris II crew of Universidad Católica del Norte for their help and support during field work. We extend our acknowledgements to the laboratory assistants of the Paleoceanography Lab at Universidad de Concepción, for their aid in sample analyses. We also wish to thank Dr. Olivier Bruguier of CNRS and his lab personnel for their assistance during ICPMs analyses. We also express our gratitude to INNOVA 07CN13 IXM-150, FONDECYT 1180413 and FONDECYT 1170408. This manuscript was mainly funded by FONDECYT Project No. 1140851. Partial support from the COPAS Sur-Austral (CONICYT PIA PFB31) and FONDAP-IDEAL centers (No. 15150003) is also acknowledged.

Tables

Table 1. Radiocarbon dates for BGGC5 and BTGC8 sediment cores collected from mixed planktonic foraminifera and monospecific benthic foraminifera (*Bolivina plicata*), respectively. The ^{14}C-AMS was performed at NOSAM-WHOI. The lab code and conventional ages collected from each core section is indicated. For error calculations see http://www.whoi.edu/nosams/radiocarbon-data-calculations.

Core identification	Material	Mass (mg)	Lab Code NOSAM	Modern fraction pMC	1σ error	Conventional Age BP	1σ error
BGGC5	Planktonic foraminifera						
10-11	Mix	1.8	OS-122160	0.8895	0.0027	940	25
18-19	Mix	1.1	OS-122141	0.7217	0.0024	2,620	25
31-32	Mix	2.7	OS-122161	0.6590	0.0021	3,350	25
45-46	Mix	2.0	OS-122162	0.6102	0.0017	3,970	25
55-56	mix	1.6	OS-122138	0.5864	0.0025	4,290	35
66-67	mix	2.8	OS-122304	0.5597	0.0018	4,660	25
76-77	mix	2.6	OS-122163	0.4520	0.0016	6,380	30
96-97	mix	1.1	OS-122139	0.4333	0.0033	6,720	60
115-116	mix	4.7	OS-122164	0.3843	0.0016	7,680	35

BTGC8	Benthic foraminifera						
5-6	Bolivina plicata	4.2	OS-130657	0.8953	0.0017	890	15
20-21	Bolivina plicata	7.7	OS-123670	0.7337	0.0021	2,490	25
30-31	Bolivina plicata	13.0	OS-123671	0.6771	0.0016	3,130	20
40-41	Bolivina plicata	11.0	OS-123672	0.6507	0.0019	3,450	25
50-51	Bolivina plicata	8.7	OS-123673	0.5877	0.0014	4,270	20
60-61	Bolivina plicata	13.0	OS-123674	0.5560	0.0018	4,720	25
71-72	Bolivina plicata	10.0	OS-123675	0.4930	0.0013	5,680	20
80-81	Bolivina plicata	7.3	OS-123676	0.4542	0.0012	6,340	20
90-91	Bolivina plicata	6.8	OS-123677	0.4259	0.0015	6,860	30
96-97	Bolivina plicata	6.8	OS-123678	0.3903	0.0013	7,560	25

Table 2. Reservoir age (DR) estimation considering the ^{210}Pb age determined with the CRS model (McCaffrey and Thomson, 1980) at a selected depth sections of the core, compared with ^{14}C ages (yr BP) from marine13.14 curve (Reimer et al., 2013), according to Sabatier et al. (2010).

Core	Depth (cm)	Age from CRS model (AD)[a]	Age years BP[b]	^{14}C age Marine 13.14	^{14}C age BP from foram.	DR
BGGC5	10.5	1828	122	499±24	940±25	441±35
BTCG8	5.5	1908	42	448±23	890±15	442±27

[a]Anno Domini
[b]Before present=1950

Table 3. Concentration of elements in Pachingo wetland sediments, considered as lithogenic background for the study area. The values correspond to mean concentrations in surface sediments (0−3 cm).

Element	**Metal/Al x 10^3**	**s**
Ca	686.5	139.3
Fe	591.3	84.5
P	8.6	0.7
Sr	5.7	0.6
Ba	5.6	0.1
Cu	0.258	0.019
Ni	0.174	0.005
U	0.020	0.003
Mo	0.020	0.003
Cd	0.0021	0.0003
Re	0.00004	0.00001

Table 4. Mean authigenic enrichment factor (EF) ± SD of trace elements calculated for Guanaqueros Bay (BGGC5 core). Lithogenic background was estimated from surface sediments of Pachingo wetland cores (see text). Age ranges were based on the variability of diatom abundance (valves g^{-1}).

Age range (cal BP)	**Diatoms ($x10^6$) (min-max)**	**Opal ($g\ m^{-2}\ yr^{-1}$) (min-max)**	**EF_U**	**EF_{Mo}**	**EF_{Re}**	**EF_{Fe}**	**EF_{Ba}**	**EF_{Cd}**	**EF_{Ni}**	**EF_{Cu}**	**EF_P**
-65 – 130	0.5 – 4.9	3 − 40	2.6 ±0.7	5.5 ±1.3	10.5 ±2.0	0.8 ±0.1	0.8 ±0.1	30.3 ±6.3	1.4 ±0.2	3.6[a] ±1.3	2.0 ±0.4
130 – 1700	0.6 – 1.7	1 – 3	5.6 ±1.4	14.5 ±3.7	18.4 ±3.8	0.9 ±0.1	0.8 ±0.1	40.6 ±3.7	1.9 ±0.1	3.0 ±0.4	2.4 ±0.4
1700 – 4500	1.9 – 5.4	2 – 21	5.5 ±0.6	14.5 ±1.5	19.8 ±2.0	0.9 ±0.1	0.8 ±0.1	55.1 ±12.2	2.3 ±0.3	3.1 ±0.5	2.2 ±0.3
4500 – 6500	2.7 – 4.5	4 − 47	5.1 ±0.8	16.9 ±3.3	19.5 ±3.0	0.9 ±0.1	0.9 ±0.1	140.1 ±46.3	3.4 ±0.5	3.1 ±0.5	3.2 ±0.5
6500 – 8400	15.7 −41.0	9 − 53	4.5 ±0.4	13.9 ±2.6	17.9 ±2.2	0.9 ±0.1	0.9 ±0.1	142.5 ±24.2	3.4 ±0.4	2.5 ±0.3	3.9 ±0.8

[a]Mean EF_{Cu} after AD 1936 was 4.6 ±0.5

Table 5. Spearman rank order correlations for geochemical data. Significant values >0.8 are indicated in bold.

BGGC5																
	Al	**P**	**K**	**Ca**	Mn	**Fe**	**Ni**	**Cu**	**Mo**	**Cd**	**Re**	**Sr**	**U**	**Ba**	**Opal**	**TOC**
Al	1.00	-0.62	0.49	-0.48	0.64	0.60	-0.75	0.56	-0.10	-0.73	-0.08	-0.33	0.08	0.49	-0.52	-0.44
P		1.00	-0.31	0.37	-0.45	-0.56	0.56	-0.57	0.01	0.61	-0.11	0.39	-0.12	-0.20	0.49	0.24
K			1.00	-0.24	**0.90**	**0.83**	-0.29	0.47	0.28	-0.42	0.33	-0.12	0.50	0.26	-0.25	-0.19
Ca				1.00	-0.47	-0.50	0.44	-0.64	0.23	0.59	0.39	**0.92**	0.30	-0.60	0.18	0.32
Mn					1.00	**0.94**	-0.51	0.68	-0.01	-0.68	0.07	-0.32	0.24	0.43	-0.39	-0.31
Fe						1.00	-0.49	**0.81**	0.03	-0.70	0.11	-0.40	0.23	0.36	-0.37	-0.21
Ni							1.00	-0.51	0.49	**0.91**	0.35	0.25	0.26	-0.70	0.72	0.64
Cu								1.00	-0.12	-0.71	-0.06	-0.61	0.00	0.31	-0.39	-0.07
Mo									1.00	0.50	**0.88**	0.10	0.91	-0.48	0.33	0.36
Cd										1.00	0.36	0.42	0.27	-0.67	0.70	0.54
Re											1.00	0.27	**0.92**	-0.50	0.16	0.38
Sr												1.00	0.24	-0.36	0.05	0.17
U													1.00	-0.39	0.10	0.29
Ba														1.00	-0.30	-0.59
Opal															1.00	0.35
TOC																1.00
BTGC8																
	Al	**P**	**K**	**Ca**	**Mn**	**Fe**	**Ni**	**Cu**	**Mo**	**Cd**	**Re**	**Sr**	**U**	**Ba**	**Opal**	**TOC**
Al	1.00	-0.19	-0.17	-0.37	-0.02	-0.03	-0.39	-0.04	-0.39	0.02	-0.13	-0.58	-0.19	0.07	-0.41	-0.29
P		1.00	0.23	0.00	0.43	0.28	0.58	0.23	0.37	0.13	-0.04	0.30	0.14	-0.14	0.56	0.13
K			1.00	-0.02	0.54	0.41	0.43	0.22	-0.11	0.05	-0.04	0.19	-0.28	0.28	0.26	0.20
Ca				1.00	-0.33	-0.27	0.00	-0.23	0.39	0.01	0.33	0.50	0.47	-0.34	0.20	0.34
Mn					1.00	0.21	0.64	0.01	0.05	0.33	0.15	0.32	-0.02	0.24	0.32	0.00
Fe						1.00	0.13	0.71	-0.40	-0.48	-0.67	-0.37	-0.62	0.13	0.14	0.10
Ni							1.00	0.24	0.56	0.20	0.25	0.64	0.19	-0.16	**0.80**	0.45
Cu								1.00	-0.25	-0.68	-0.56	-0.22	-0.61	-0.10	0.21	0.37
Mo									1.00	0.45	0.59	0.66	0.69	-0.41	0.58	0.30
Cd										1.00	0.56	0.39	0.52	0.11	0.10	-0.12
Re											1.00	0.53	**0.83**	-0.16	0.13	0.17
Sr												1.00	0.58	-0.13	0.52	0.23
U													1.00	-0.19	0.21	0.00
Ba														1.00	-0.28	-0.42
Opal															1.00	0.39
TOC																1.00

Figures

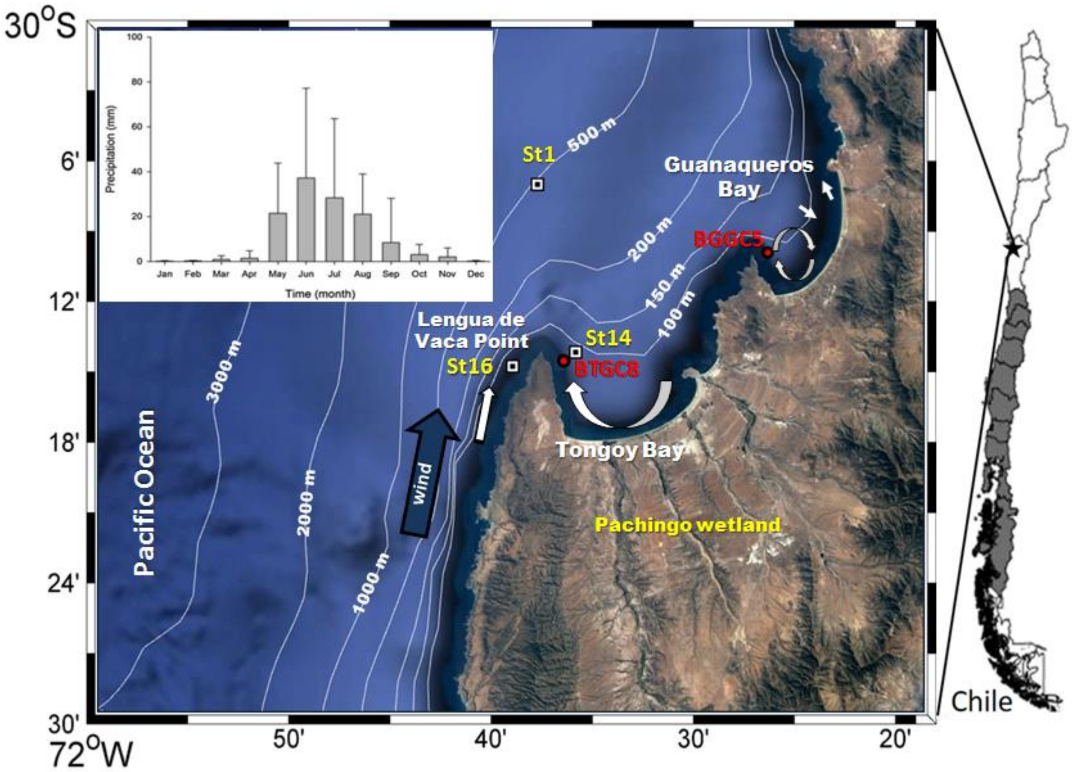

Figure 1. Study area showing the position of sampling stations. Sediment cores were retrieved from Guanaqueros Bay (BGGC5) and from Tongoy Bay (BTGC8) at water

depths of 89 and 85 m, respectively. Information of dissolved oxygen (DO) in the water column at ST1and ST16 and of suspended organic particles collected at ST14 sampling sites was gathered in a previous project (INNOVA 07CN13 IXM-150). Monthly precipitation in mm (bars) (means ± SD; Montecinos et al., 2016). Schematic representation of the bays circulation (white arrows) and wind direction is indicated (blue arrow) obtained from Valle-Levinson and Moraga-Opazo (2006) and Moraga-Opazo et al. (2011).

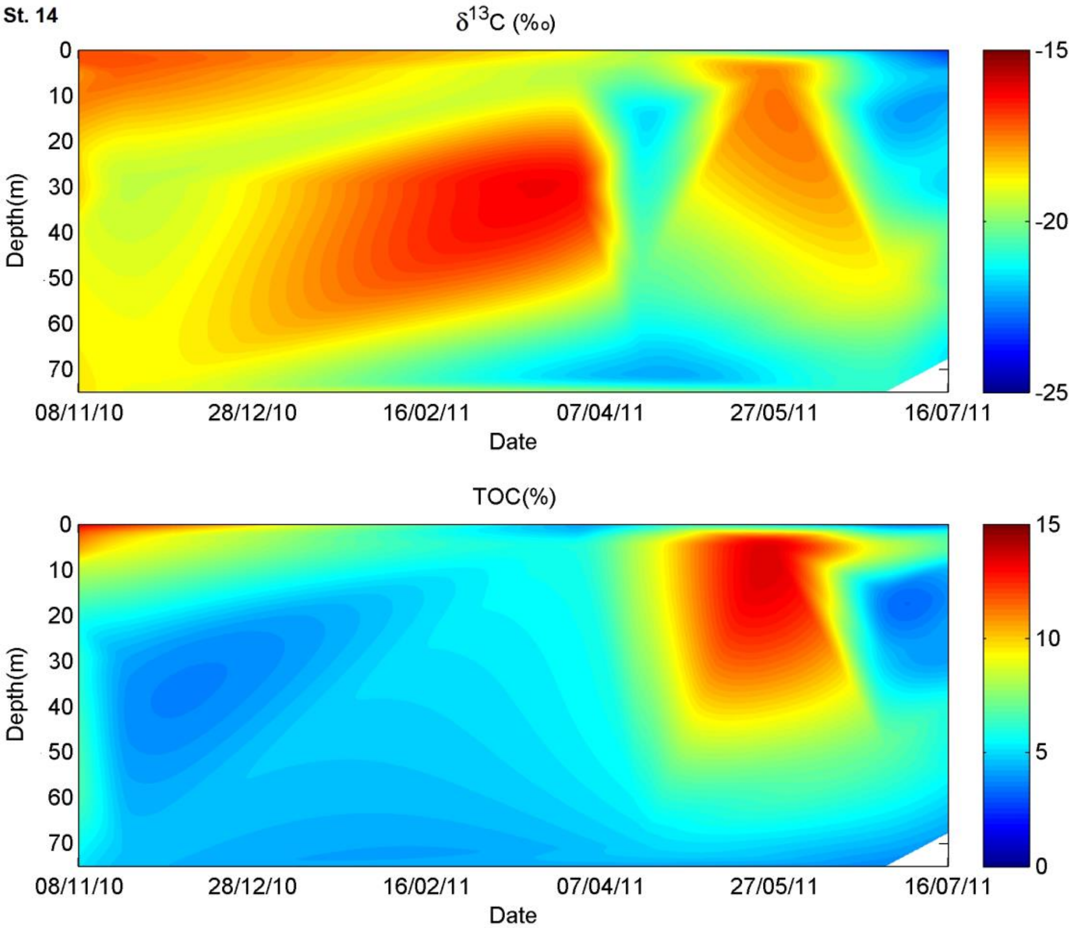

Figure 2. Suspended particulate matter composition (TOC % and δ^{13}Corg) measured in the water column between October 2010 and October 2011, at station St14, Tongoy Bay, Coquimbo (30°S).

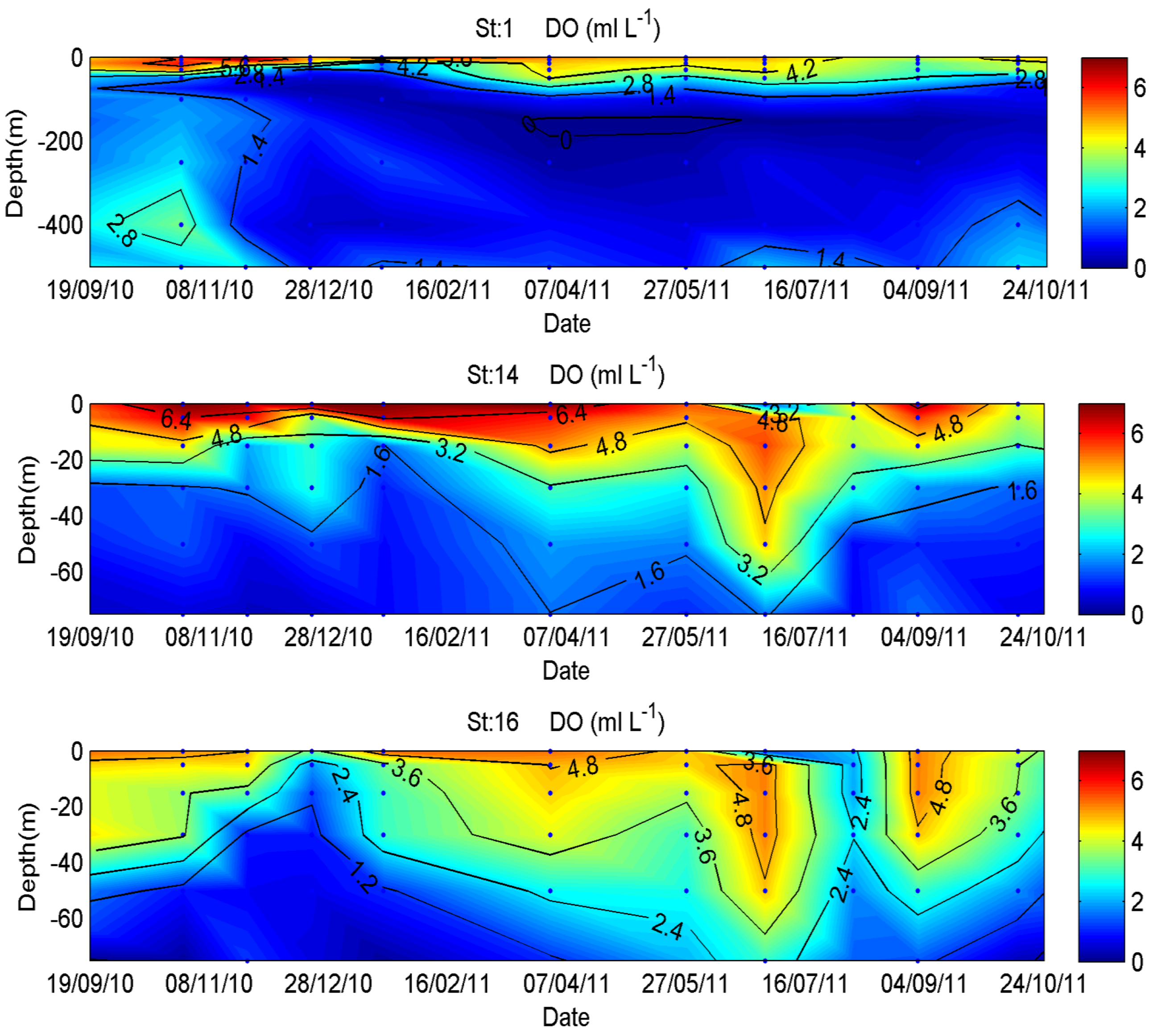

Figure 3. Dissolved Oxygen (DO) time series in the water column measured between October 2010 and January 2011, at stations St1, St14 and St16 off Tongoy Bay, Coquimbo (30°S).

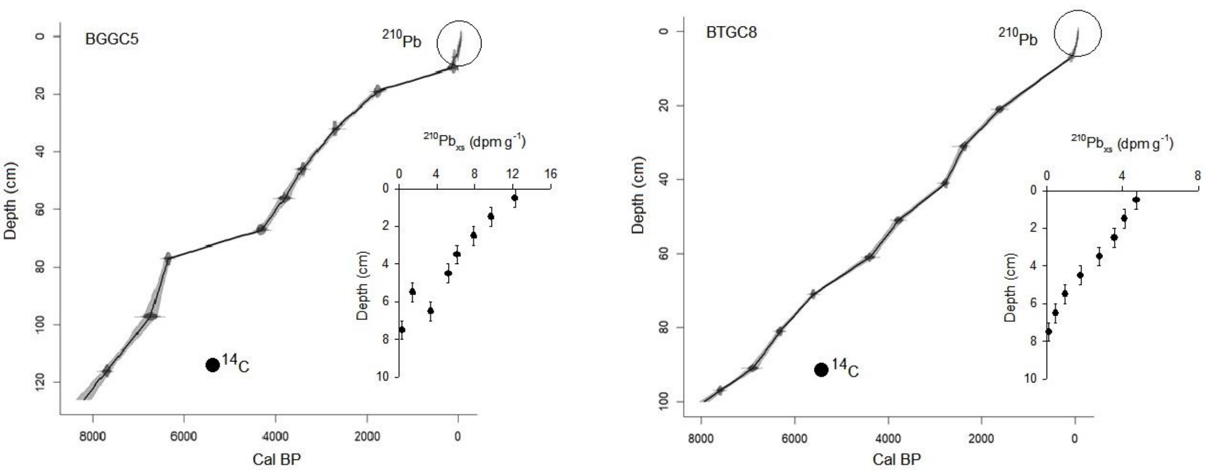

Figure 4. Age model based on ^{14}CAMS and ^{210}Pb measurements. The time scale was obtained according to the best fit of curves of $^{210}Pb_{xs}$ and ^{14}C points using CLAM 2.2 software and Marine curve ^{13}C (Reimer et al., 2013).

a) BGGC5

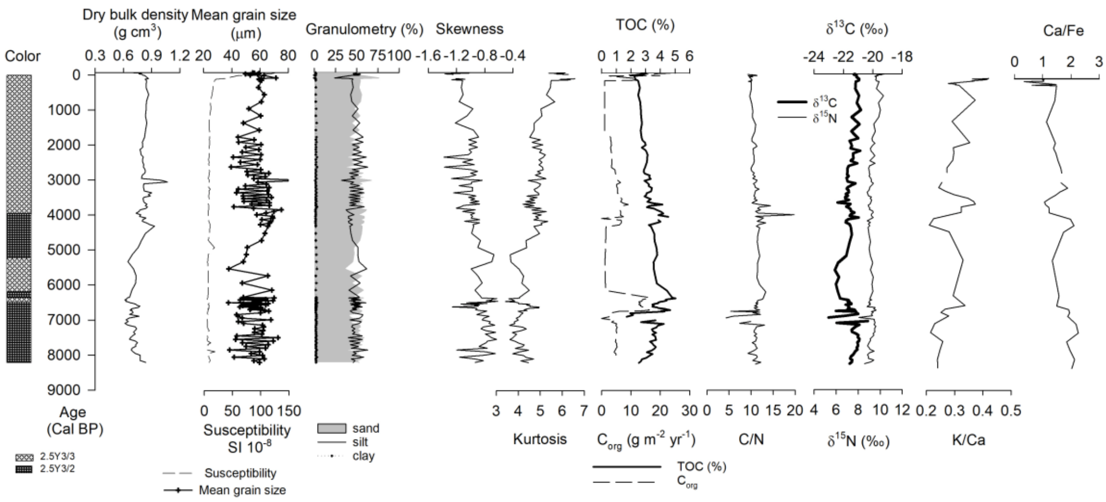

b) BTGC8

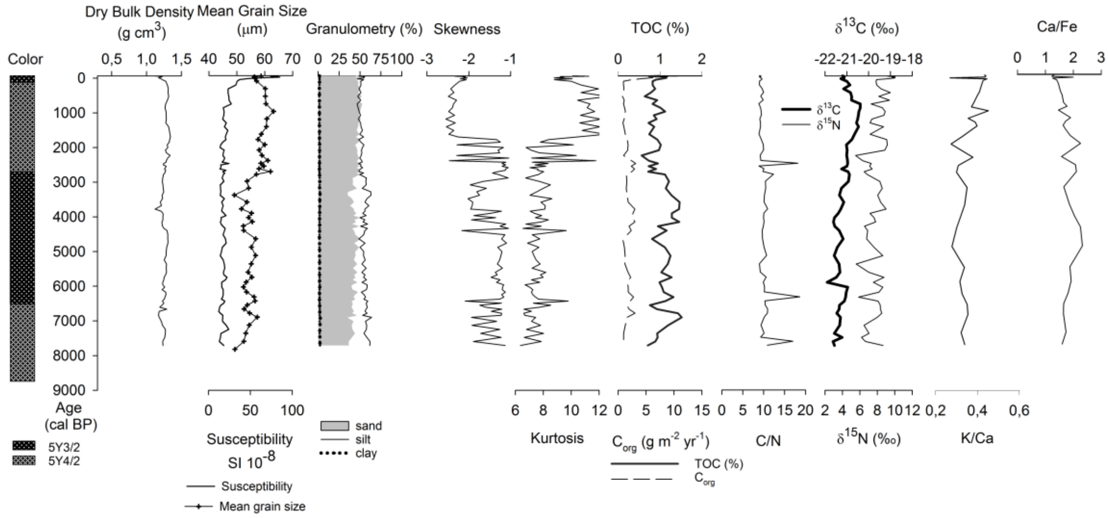

Figure 5. Characterization of sediment cores retrieved from (a) Guanaqueros Bay (BGGC5) and (b) Tongoy Bay (BTGC8), where is shown the color (Munsell chart scale) in depth, dry bulk density, mean grain size, granulometry (% sand, silt and clay), statistical parameters (skewness, kurtosis), organic components (TOC, C/N ratio, stable isotopes δ^{15}N and δ^{13}C) and chemical composition (K/Ca, Ca/Fe).

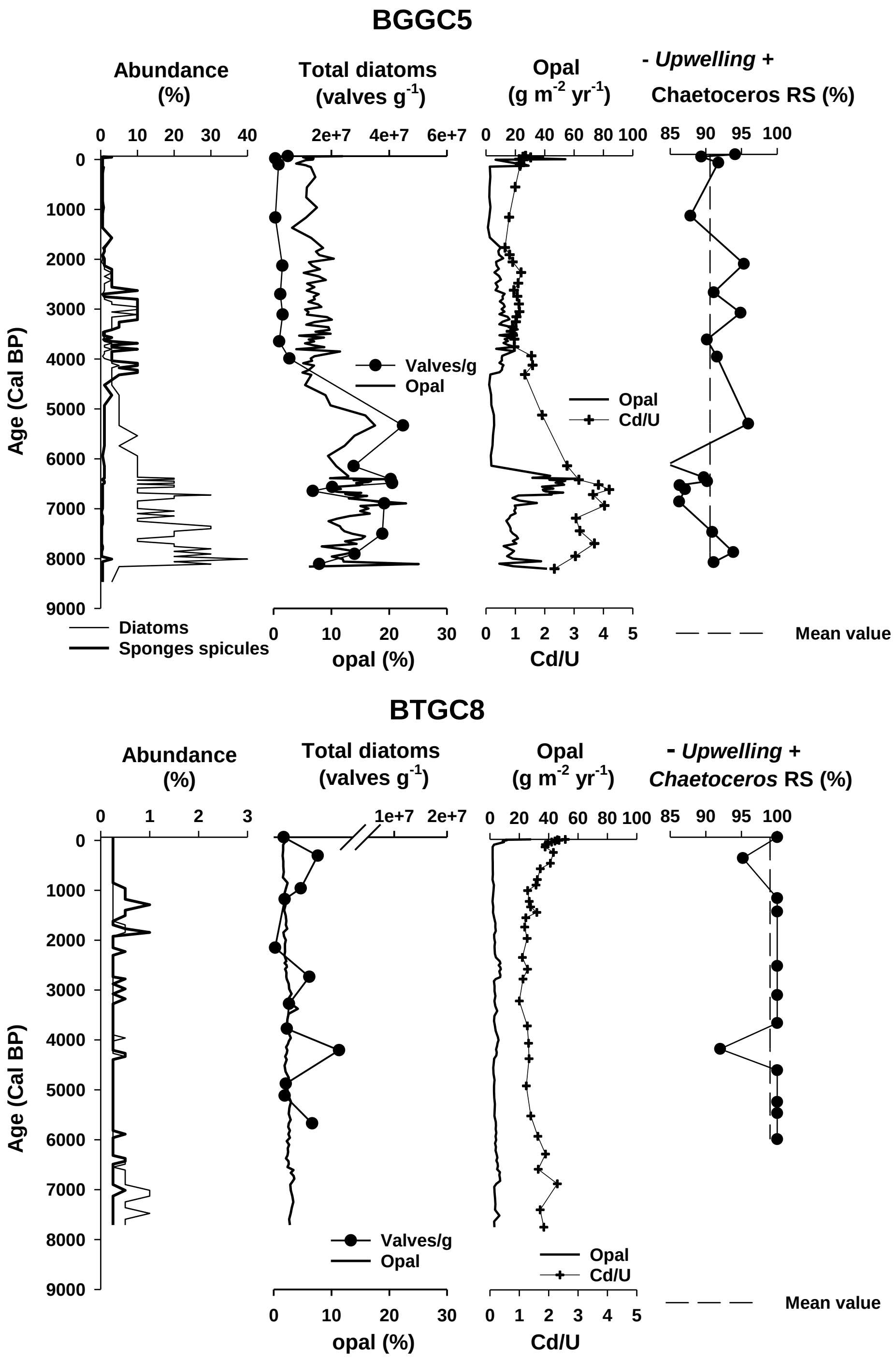

Figure 6. Diatom and sponge spicules' relative abundances, total diatom counts (valves g^{-1}) and opal (%), opal accumulation (g m^{-2} yr^{-1}), and Cd/U ratio, and downcore variations in *Ch.* resting spores percentages as proxy of upwelling intensity in BGGC5 and BTGC8 cores (Guanaqueros and Tongoy Bay, respectively), the medium dash line represents the average of *Ch. resting* spore for the respective core. Cd/U distribution was included as a proxy for redox condition.

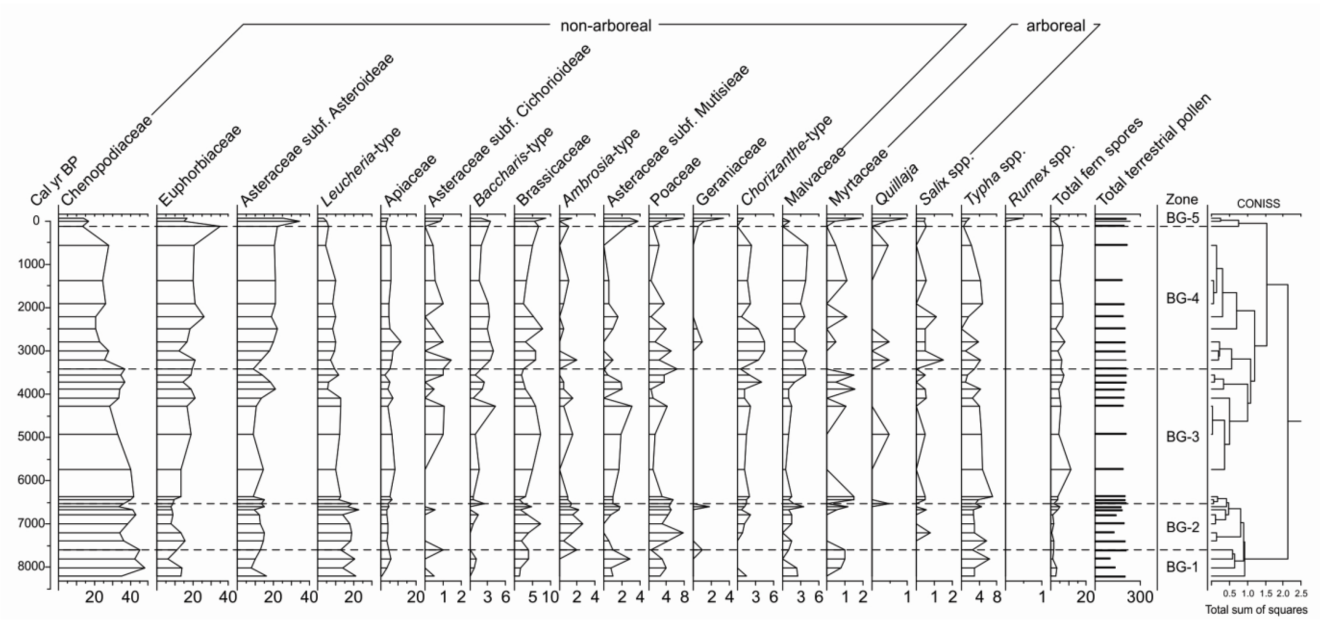

Figure 7. Pollen record in BGGC5 core.

a) BGGC5

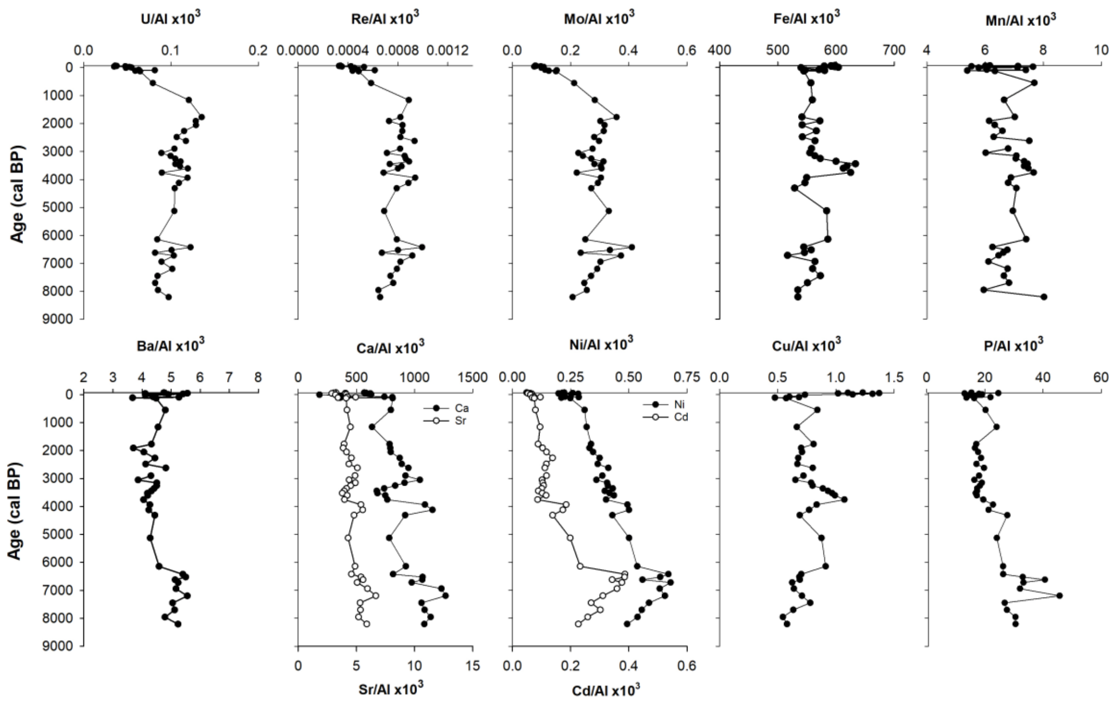

b) BTGC8

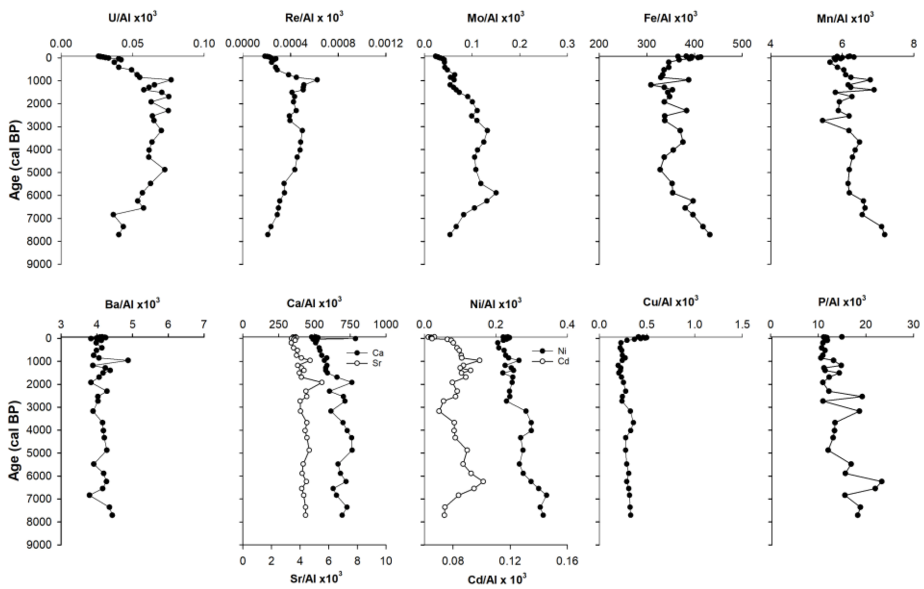

Figure 8. Downcore trace element variations on: (a) Guanaqueros Bay (BGGC5) and (b) Tongoy Bay (BTGC8), off Coquimbo (30°S).

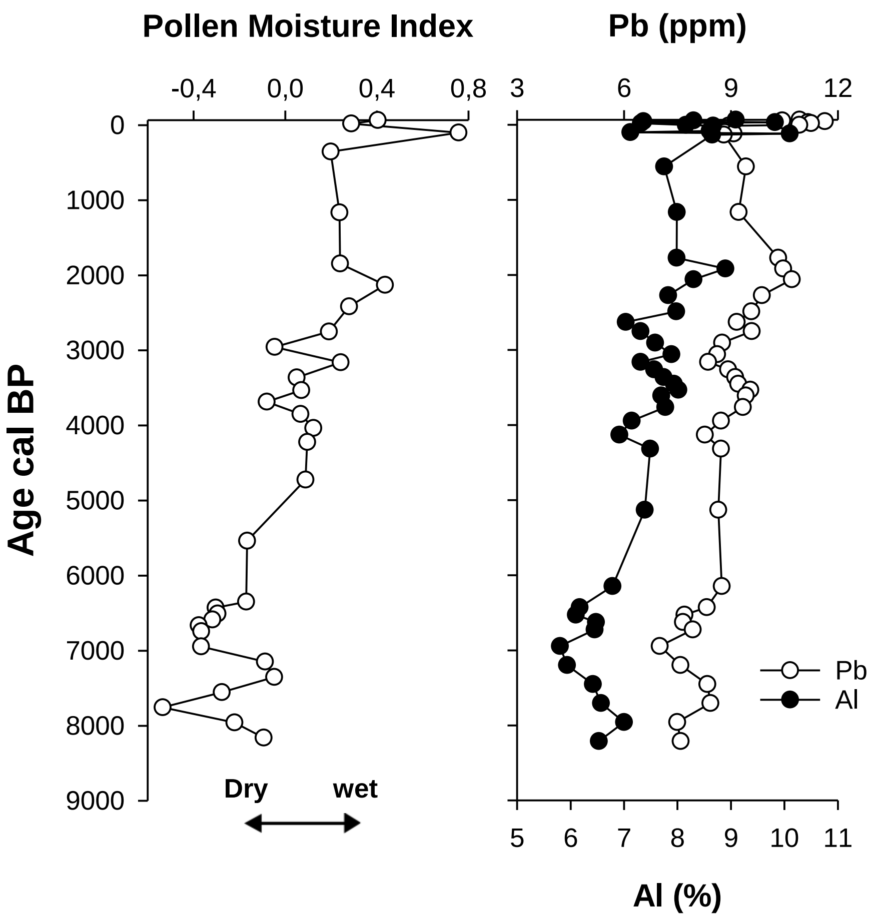

Figure 9. Pollen Moisture Index defined as the normalized ratio between Euphorbiaceae (wet coastal shrub land) and Chenopodiaceae (arid scrubland). Positive (negative) values for this index indicate the relative expansion (reduction) of coastal vegetation under wetter (drier) conditions. Pb and Al distribution at BGGC5 core, representatives of terrigenous input to the bay.